LASER INTERFEROMETER GRAVITATIONAL WAVE OBSERVATORY
- LIGO -
CALIFORNIA INSTITUTE OF TECHNOLOGY
MASSACHUSETTS INSTITUTE OF TECHNOLOGY

Technical Note	**LIGO-T2100205–v1**	2021/09/19

LIGO Laser Beam Tracking

SURF Student: Anirban Bairagi
Mentors: Yehonathan Drori, Tega Edo, Rana Adhikari

California Institute of Technology
LIGO Project, MS 18-34
Pasadena, CA 91125
Phone (626) 395-2129
Fax (626) 304-9834
E-mail: info@ligo.caltech.edu

Massachusetts Institute of Technology
LIGO Project, Room NW22-295
Cambridge, MA 02139
Phone (617) 253-4824
Fax (617) 253-7014
E-mail: info@ligo.mit.edu

LIGO Hanford Observatory
Route 10, Mile Marker 2
Richland, WA 99352
Phone (509) 372-8106
Fax (509) 372-8137
E-mail: info@ligo.caltech.edu

LIGO Livingston Observatory
19100 LIGO Lane
Livingston, LA 70754
Phone (225) 686-3100
Fax (225) 686-7189
E-mail: info@ligo.caltech.edu

http://www.ligo.caltech.edu/

Contents

1 Introduction

Gravitational Waves are produced by the bulk accelerated motion of matters, that propagates as waves in the fabric of spacetime at the speed of light. The existence of Gravitational Waves were first predicted by Albert Einstein in 1916 as a consequence of his work on General Relativity. The LIGO interferometers were built using the basic idea of Michelson interferometer and its precise strain measurements rely on the laser beam resonators in the optical cavity of the interferometers. Many years of relentless efforts and several technical upgradations in the detectors made by the scientists helped aLIGO to achieve the sensitivity to detect more than 50 GW events till date.

When the GW passes through the interferometer its arm length increases and decreases consecutively which causes change in differential arm length during the event. The intensity of the recombined light at the detector readout which is a function of the differential arm length (DARM) of the interferometer, gives the infinitesimal gravitational wave strain as shown in Figure 1. The LIGO detector is highly susceptible to various kind of noises which are basically unwanted signal produced by interactions among detector subsystems or with the surrounding environment that gets added to the GW strain data. Here, we are interested in the Fabry-Perot cavity and test masses of the detector. In this project we are trying to detect the position of the laser beam spot on the test masses. The aLIGO is not free from scattered light noise. The scattering of light helps us to see the scattered beam spot from any angle on the mirror surfaces. Due to irregularities and point scatterers of the mirror, the light undergoes deflection from its path defined by specular reflection and hence scattering occurs. The angular motion of the mirrors causes oscillatory translational motion of the beam spot on the mirror. Thus, tracking the position of the beam has become one of the important task within LIGO community.

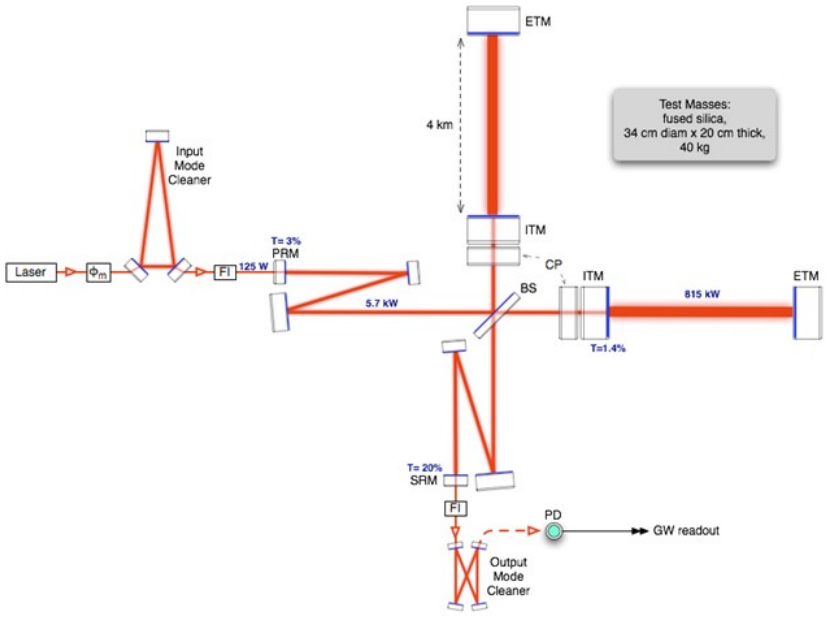

Figure 1: Schematic Diagram of LIGO detector

One should not observe the beam spot ideally when it is viewed at an angle to the beam axis since no light deflects according to the laws of specular reflection. However, due to scattering of light the beam spot can be observed from different angles with varying intensities according to the Bidirectional Reflection Distribution function (BRDF) of the mirror.

$$\mathrm{BRDF} = \frac{\mathrm{P}_s/\Omega}{\mathrm{P}_i \cos\theta_s} \tag{1}$$

where P_i and P_s are incident and scattered power and θ_s is the scattering angle and Ω is the solid angle subtend at the CCD camera used for capturing the image of the test mass. We are mostly interested in large angle scattering where the optic behaves as a Lambertian surface. Here Basler ace acA640-120gm camera equipped with a Gigabyte Ethernet (GigE) interface has been installed for faster data transmission over ethernet network as shown in Figure 2. Two lens telescope system is placed between GigE camera and mirror to focus the beam spot onto the GigE camera sensor while ensuring lenses and camera are placed perpendicular to scattered beam axis and optimum utilization of the CCD pixel arrays. It gives the videos of the scattered light coming from the surface of the test masses.

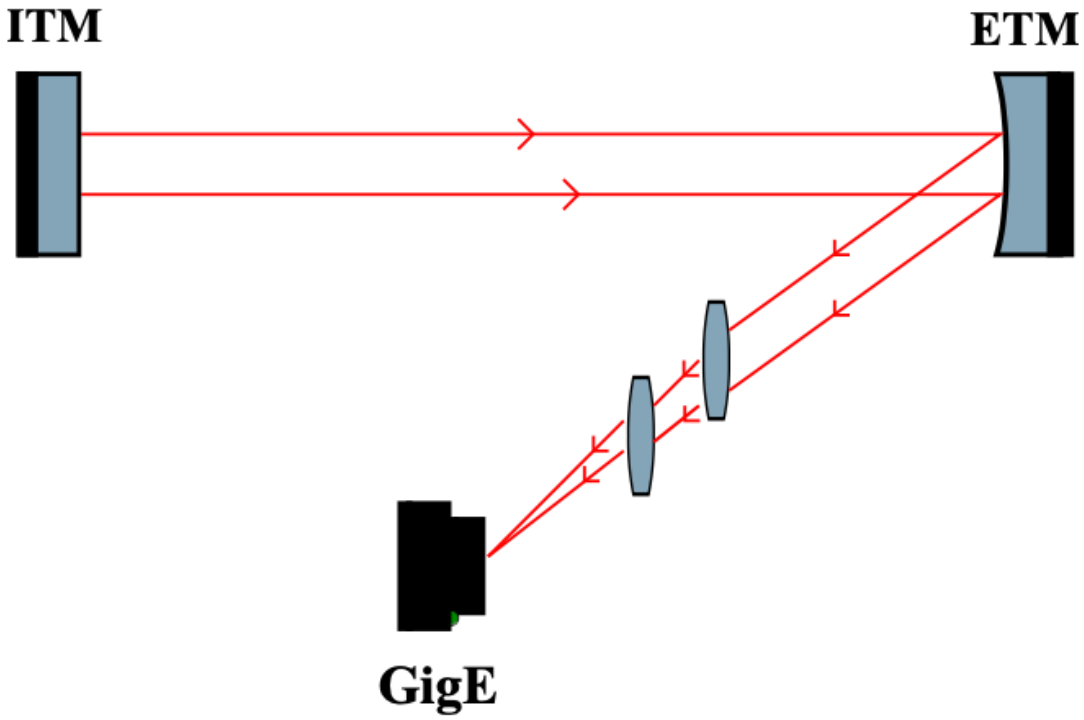

Figure 2: GigE camera setup for imaging the scattered light

Pooja Sekhar, Milind Vaddiraju have already tried some classical image processing techniques which failed to detect the centroid of the beam because the beam do not retain its gaussianity after scattering due to irregularities of the mirror surface. In Figure 3[2], on plotting the intensity vs pixel number along a particular axis of the image of the beam spot, the intensity profile deviates quite a bit from the expected Gaussian profile. This is caused due to the scattering from point defects.

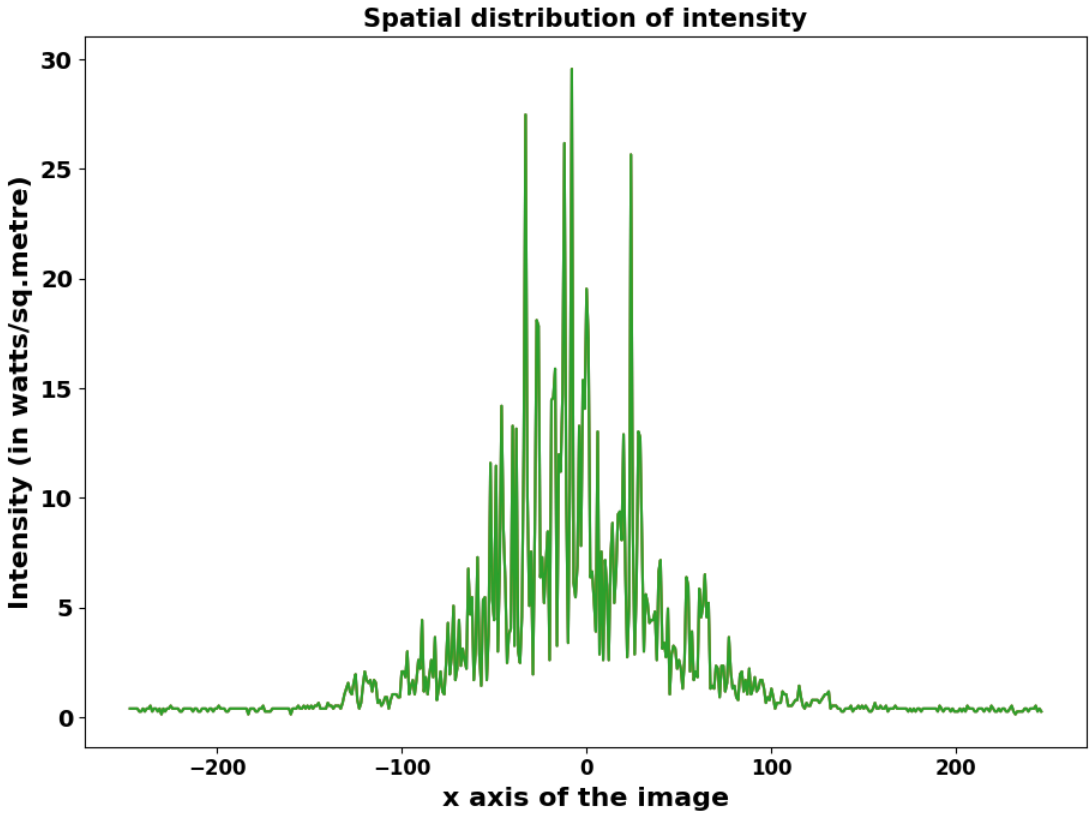

Figure 3: Deviation from Gaussian intensity profile

Several attempts made by them using Neural Networks has shown reasonable good results in comparison to the classical methods. Neural networks were trained with hyperparameters tuned using a grid search and beam spot motion at 0.2 Hz with an amplitude of about 3mm is tracked with maximum error under 20% [1]. But we require better accuracy for our purpose.

2 Motivation

These are future goals of GW researchers for which our current work on laser beam tracking is very crucial. We need to detect the position of the beam spot to understand the angular movement of the mirror so that feedback control system attached to the test masses fix its position as shown in Figure 4.

3 Objective

Our main objective is to get the position of the beam spot at every instances with better accuracy using some traditional image processing techniques along with some Deep Learning models. Although we will be stick to detecting the position only in this work, but in future it will help in reducing some noise from the data and analysing the motion in a better way if we become successful.

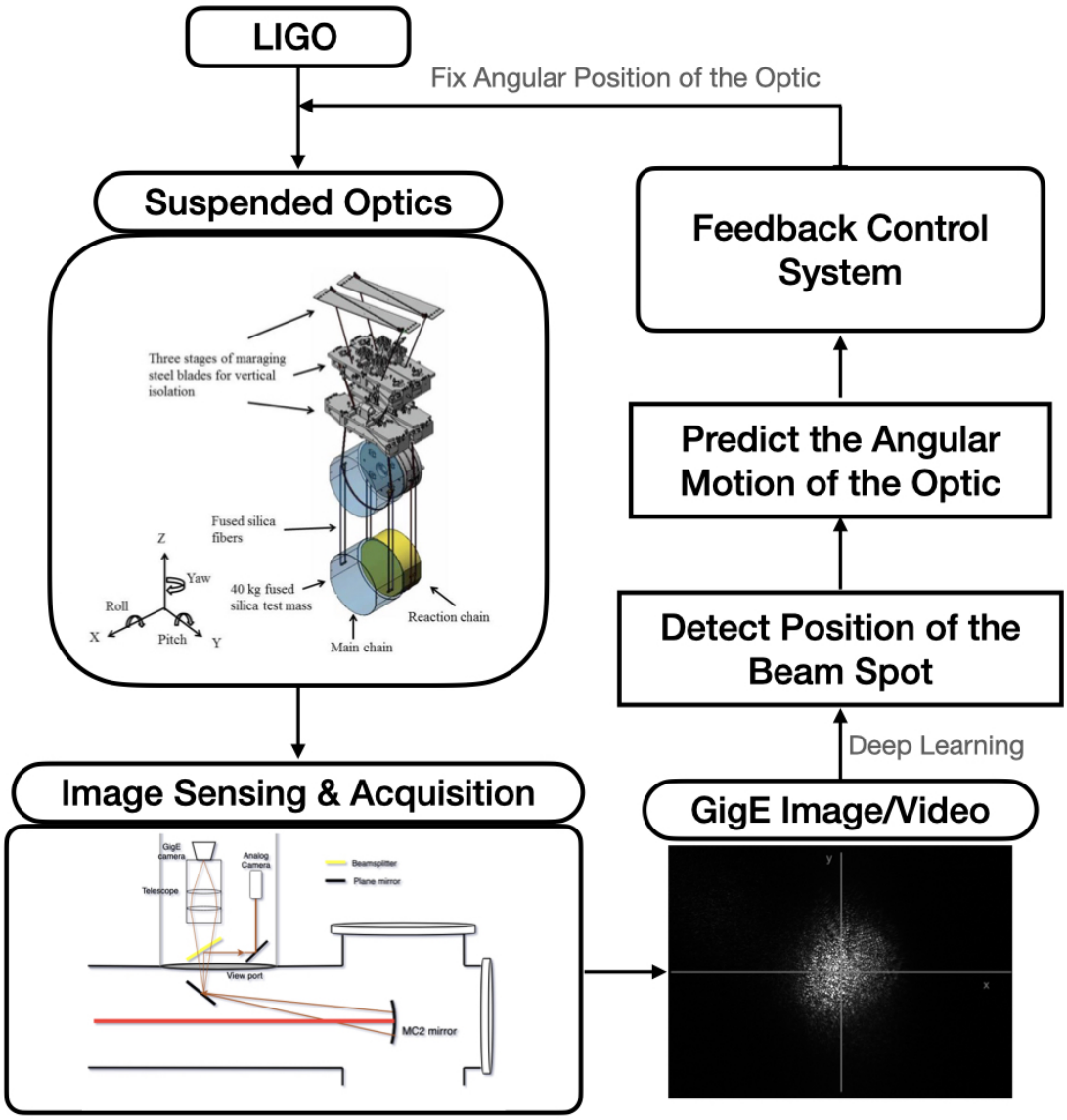

Figure 4: Angular Control of Suspended Optics

- Generate simulated video of beam spot motion. Since Deep Learning models are expected to produce better results and we lack labelled image datasets for training, we need to simulate scattering light images comparable to the GigE images.
- Develop a Convolutional Neural Network (CNN) model to extract features from the images i.e. finding the centroid of the beam and angular deflection of the mirror.

4 Simulation of Beam Spot

4.1 Purely Gaussian Beam

Here we will consider a fundamental laser beam with a linearly polarized, Gaussian field distribution in the beam waist

$$\vec{\mathbf{E}}(x', y', 0) = \vec{\mathbf{E}}_0 e^{-\frac{(x'-\mu_x)^2+(y'-\mu_y)^2}{w_0^2}} \tag{2}$$

where E_0 is constant field vector in the transverse (x,y) plane and (μ_x, μ_y) is the position of the centroid of the beam on the plane.

$$\tilde{\mathbf{E}}(k_x, k_y, 0) = \frac{1}{4\pi^2}\int_{-\infty}^{\infty}\int_{-\infty}^{\infty}\vec{\mathbf{E}}(x', y', 0)e^{-i(k_x x'+k_y y')}dx'dy' \tag{3}$$

$$\tilde{\mathbf{E}}(k_x, k_y, z) = \tilde{\mathbf{E}}(k_x, k_y, 0)e^{ik_z z} \tag{4}$$

Then, the field at the object plane becomes

$$\vec{\mathbf{E}}(x, y, z) = \int_{-\infty}^{\infty}\int_{-\infty}^{\infty}\tilde{\mathbf{E}}(k_x, k_y, z)dk_x dk_y \tag{5}$$

The intensity of the beam i.e. $\mathrm{I}(x, y, z) = \vec{\mathbf{E}}^{\star}\vec{\mathbf{E}}$ will give the image of the beam spot shown in Figure 5(left).

4.2 Scattered Beam

Using these equation we can construct beam spot centred at (μ_x, μ_y) at any irregular mirror surface by varying the z over the surface. Now the difference between the field for varying z and field for constant z gives the field of scattered light.

Suppose, the mirror surface is at an approximate distance z from the source plane. Then, the electric field of the scattered will be

$$\vec{\mathbf{E}}_{\text{scatter}}(x, y, z) = \vec{\mathbf{E}}(x, y, z)e^{ik_z\Delta z} - \vec{\mathbf{E}}(x, y, z) \tag{6}$$

where $\Delta z(x, y)$ is the height of irregularities on the mirror surface. For the places of no irregularities on the mirror $\Delta z = 0$.

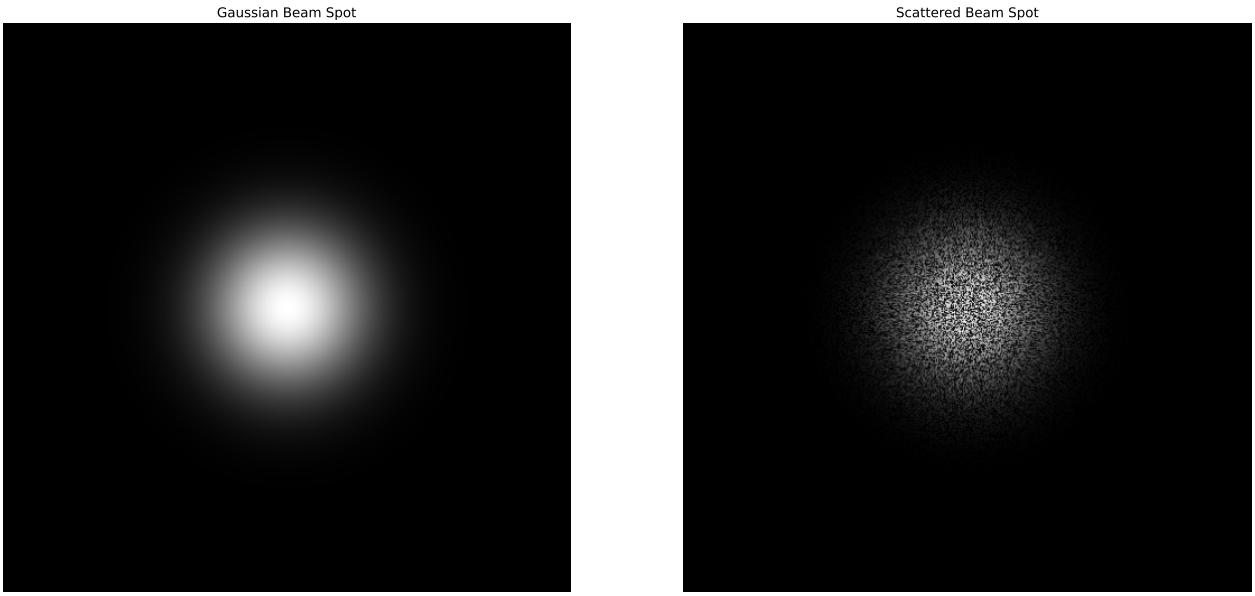

Figure 5: These images of resolution 512x512 are generated on a 34 cm x 34 cm camera for a gaussian laser beam of radius 6.5 cm

Thus, the intensity of the scattered light is

$$\mathrm{I}_{\mathrm{scatter}}(x, y, z) = \vec{\mathbf{E}}^{\star}_{\mathrm{scatter}} \vec{\mathbf{E}}_{\mathrm{scatter}} \tag{7}$$

Using these formulation we can simulate beam spot as shown above in Figure 5(right).

5 Noise

From the scattered power of the laser beam spot we can get number of photons generated per second by dividing the average power by the energy of a single photon of wavelength λ.

$$p = \frac{\mathrm{P}_s}{hc/\lambda}$$

If a lens of 2" diameter has been placed at a distance of 1 meter from the ETM and making angle of 10° to the beam axis as shown in Figure 2, the solid angle subtended at the CCD camera will be, $\Omega = \int \sin\theta d\theta d\phi$=0.0256

For a laser power of 500 kW inside the Fabry-Perot cavity and the mirror surface being Lambertian for large angle scattering i.e. BRDF=$\frac{1}{\pi}\mathrm{sr}^{-1}$ the scattered power is obtained from Eq. 1,

$$\mathrm{P}_s = \mathrm{BRDF} \times \Omega \mathrm{P}_i \cos\theta_s = \frac{1}{\pi} \times 0.0256 \times 5 \times 10^5 \times \cos 10^\circ = 4022.15\mathrm{W} \tag{8}$$

So, for a 1064 nm wavelength laser the number of photons incident on the camera will be, $p = 2.15 \times 10^{22}$

Now the number of e^- generated per pixel per second is proportional to the number photons stored in the pixel

$$N = \frac{dN}{dp} \times p$$

where $\frac{dN}{dp}$ is the photon to electron conversion rate in the CCD camera. But this is not perfectly true for all values of p. Below a certain threshold value of p, N is just the number of electrons contributing to the Dark Current noise and above some value of p, the number of electrons at each pixel reach a saturation point resulted a saturation in intensity.

5.1 Shot Noise

Shot noise originates due to the discrete nature of photons i.e. same number of photons can not generate same number of photo-electrons each time. The fluctuation follows Poisson statistics and therefore, shot noise is equivalent to $\sqrt{N}$. Shot noises for various simulation models have been shown below considering 2.15×10^{20} photons have been incident on the CCD camera for a exposure time of 10 ms assuming photon to electron conversion rate is 0.8.

(a) Shot noise added to Gaussian Beam

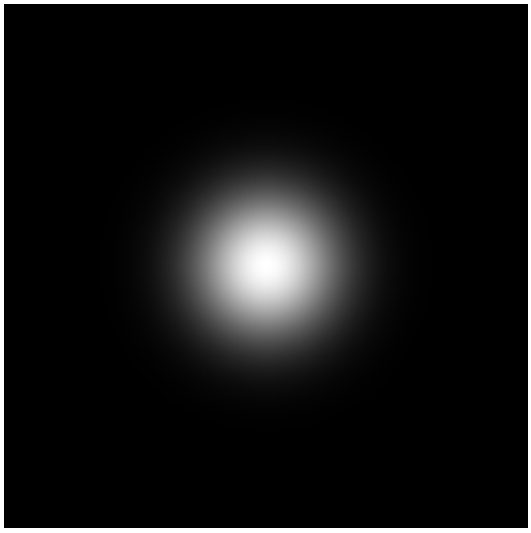

(b) Shot noise added to Scattered Beam

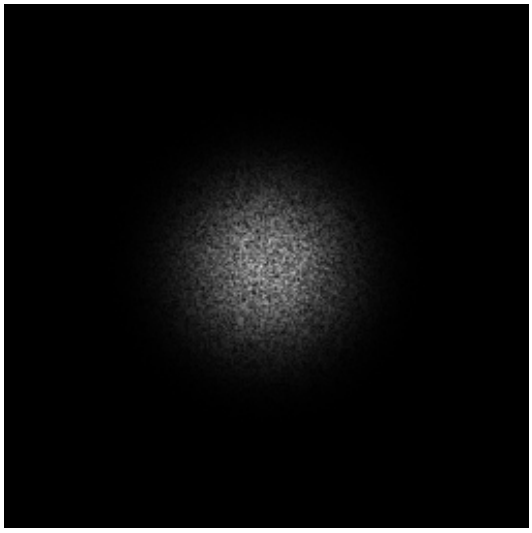

Figure 6:

5.2 Dark Current Noise

Dark current noise is generated due to the electrons that are produced thermally within the silicon structure of CCD which is independent of the photon induced signal. Cryogenics helps in reducing the temperature within the cavity and hence reduces the dark current up to several orders. Like Shot noise, Dark Current noise follows Poisson relationship and is equivalent to the square root of number of thermal electrons generated within the image exposure time.

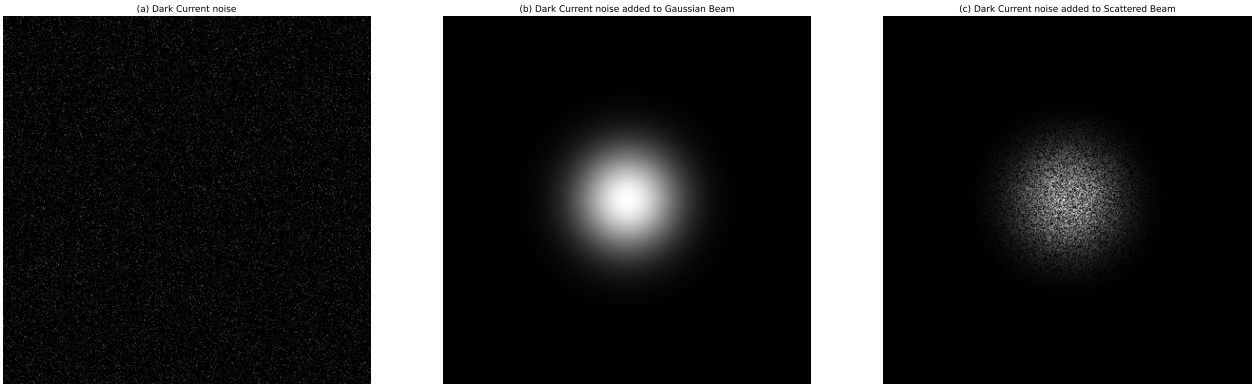

Figure 7: (a) Dark Current noise for dark current of 11 electron per pixel per second for a exposure time of 10 ms [3], (b) Image of the gaussian beam spot considering dark current, (c) Image of the scattered beam spot considering dark current

5.3 Photon Saturation effect

After a certain threshold value of number of photon incident on each pixel, the number of photo-electrons do not increase hence the intensity at such pixels get saturated. Here we have assumed this threshold value is of the order of 10^{16}

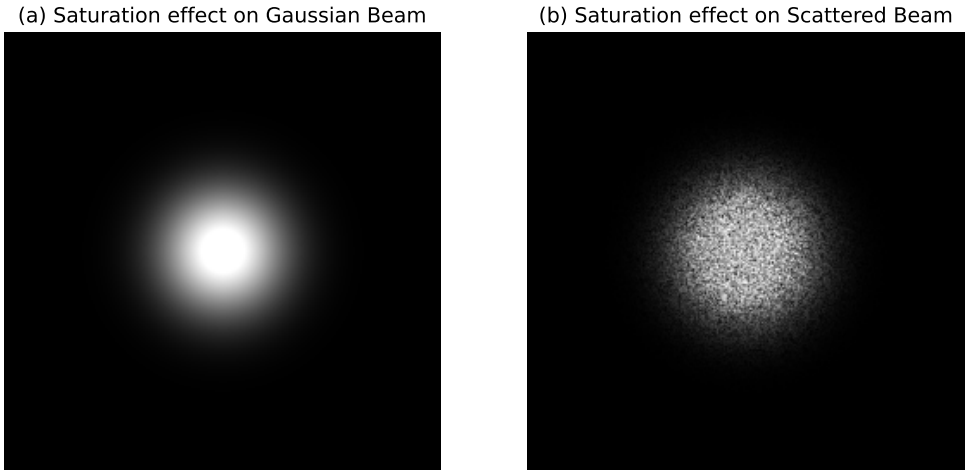

Figure 8:

6 Data Generation

Data preparation is one of the important steps in any Supervised Learning problem. Here we will be generating images of beam spot corresponding to a predefined beam motion on the mirror based on each of these following simulation models:

- Gaussian Beam [5]
- Scattered Beam [5]
- Gaussian Beam with CCD Noise [8]
- Scattered Beam with CCD Noise [8]

Considering there types of motion (i.e. along X axis only, along Y axis only, along both direction) Train, Validation and Test set have been prepared. For all of these cases we will be taking a CCD screen of $34 \times 34\text{cm}^2$ and beam radius 6.5 cm and all of the images have 512×512 resolution.

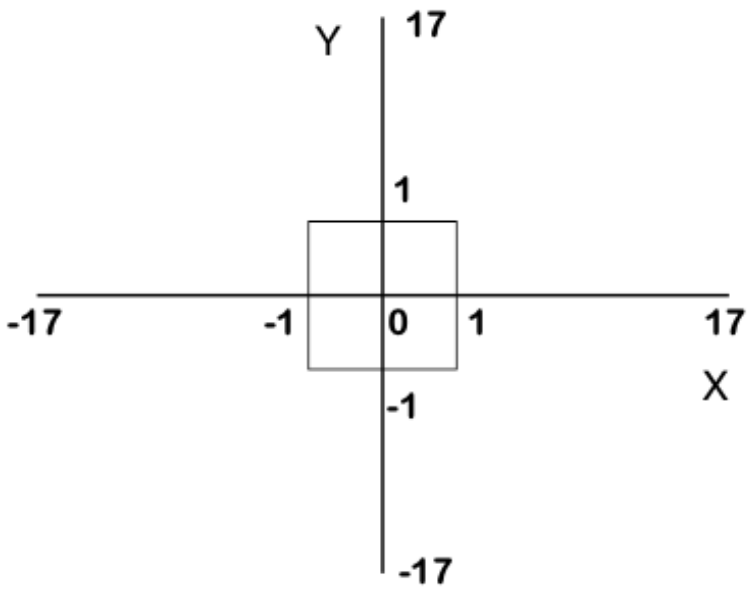

Figure 9: Defining coordinate system on CCD screen

6.1 One Dimensional Motion: Movement along X-axis/ Y-axis only

Now we will show beam position on X or Y axis at different times in our datasets which we are going to use.

Train Data:

We are taking uniformly separated data points on the axis between -1 cm and 1 cm as centroid position of our generated beam spot images [10]. Our simulated video is of 20 secs duration with 32 fps.

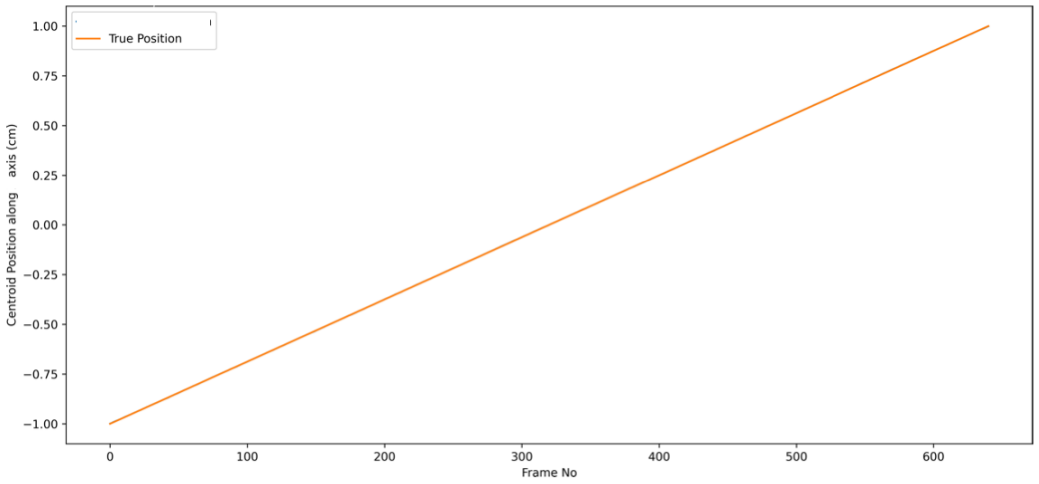

Figure 10: Position of beam at different times for consecutive frames

Validation Data:
For generating validation data we will be taking superposition two sinusoidal waves of frequency 0.2 Hz and 0.4 Hz and of amplitude 0.5 cm each for a time period of 10 sec with 32 fps.

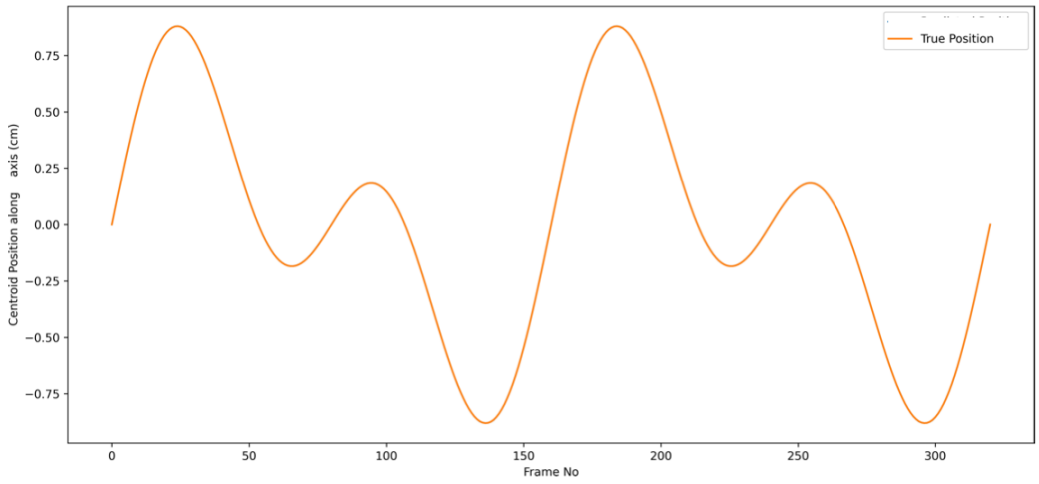

Figure 11: Position of beam at different times for consecutive frames

Test Data:
Here we will superpose two sinusoidal waves of frequency 0.1 Hz and 0.2 Hz and of amplitude 0.5 cm each for a time period of 10 sec with 32 fps.

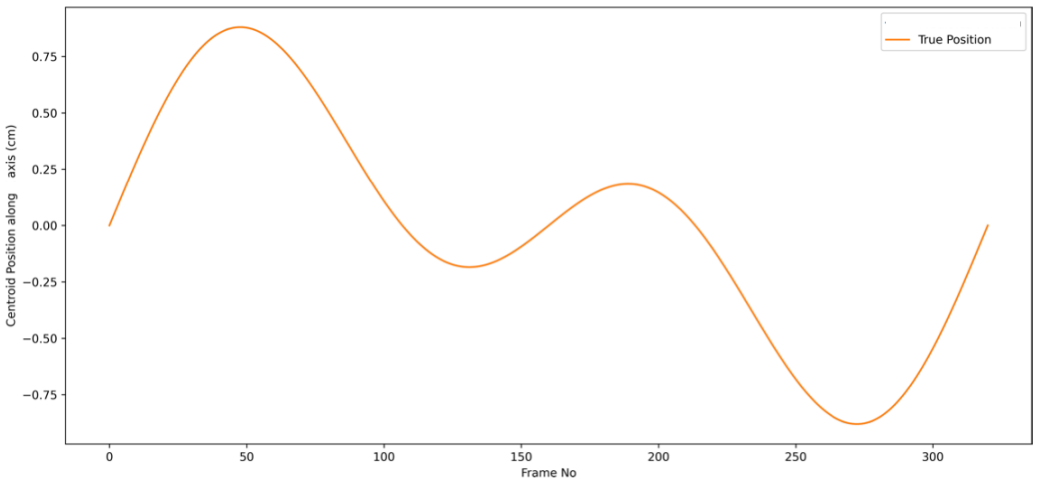

Figure 12: Position of beam at different times for consecutive frames

6.2 Two Dimensional Motion: Movement on X-Y plane

In this case we will be taking 2D motion of the beam spot on X-Y plane of mirror and corresponding beam positions at various times have been shown below.
Train Data:
Here we have generated 32×32 meshgrid on $2 \times 2\text{cm}^2$ area of CCD screen centered at origin. Here beam is moving along +ve X axis and after completing one axis it moves to next Y position and starts moving towards +ve X direction.

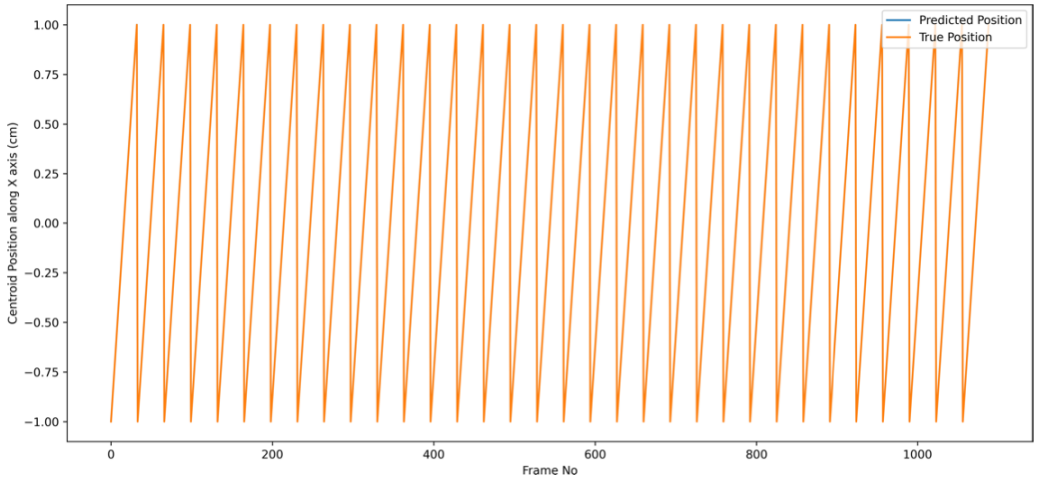

Figure 13: X coordinate of the beam spots

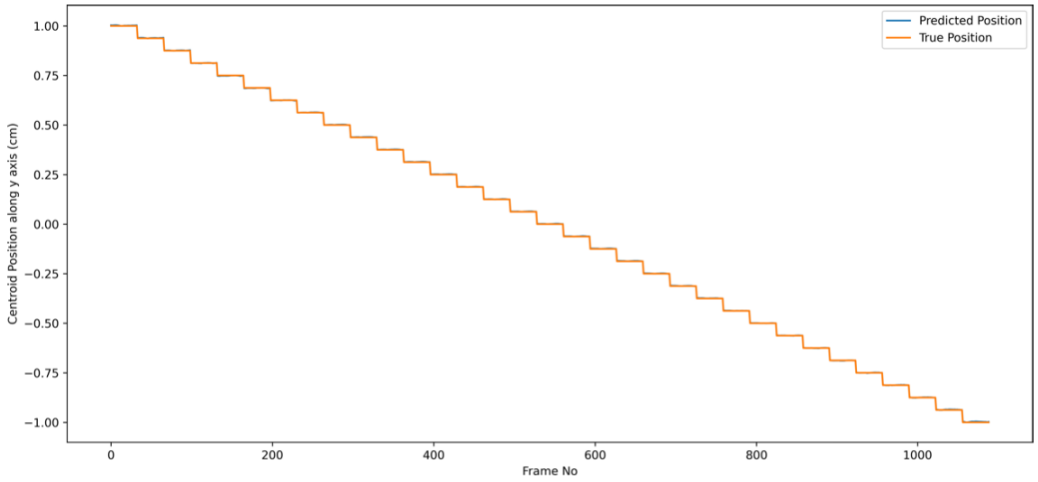

Figure 14: Y coordinate of the beam spots

Validation and Test Data:
Here our beam movenment along X axis is similar to 11 and 12 respectively but Y axis movement is sinusoidal with frequency of 0.1 Hz and amplitude of 1 cm.

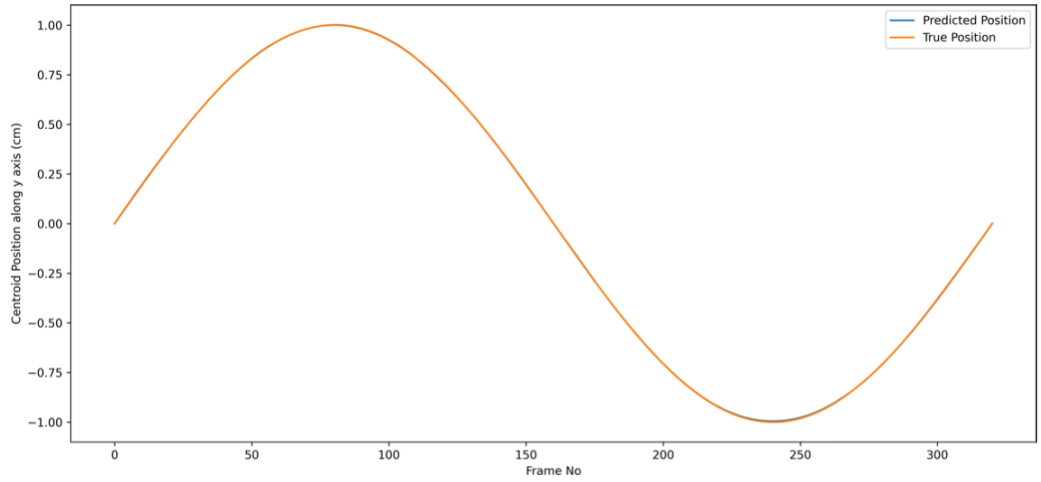

Figure 15: Y coordinate of the beam spots

7 Convolutional Neural Network

Convolutional neural network is a special type of machine learning algorithm which is mainly used to extract complex features from images. 1D convolution is exception which is used on any timeseries data instead of images.

It consists of several convolution operations, maximum or average pooling, activation layer etc as shown below.

7.1 Model Architecture

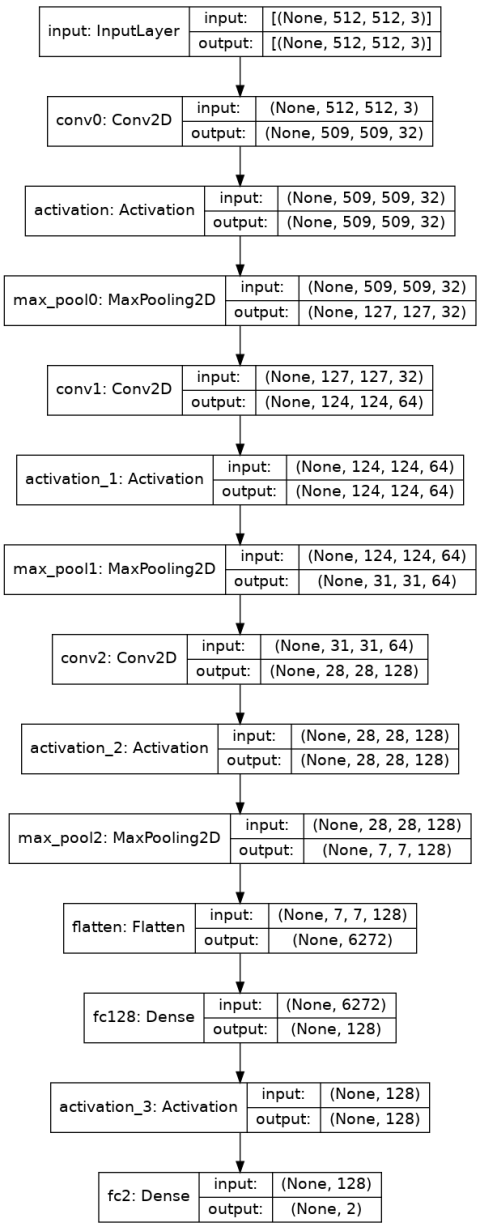

Figure 16: CNN Model Architecture

When this model will be applied on any beam spot image it will try to predict its position by giving two values corresponding to x and y coordinate of its centroid.

7.2 Cost Function

Mean Squared Error (MSE) is our preferred choice of cost function for this problem. It gives the MSE loss of the predicted position and true position of the beam spot i.e. the lesser loss indicates better model for centroid detection.

$$\textbf{Mean Squared Error} = \frac{\sum_{\text{Frame no}=1}^{N} (\text{Predicted Position - True Position})^2}{\text{Total no. of Frames}} \tag{9}$$

7.3 Metric

Metric is a measure of the goodness of any Machine Learning model. Here we will be using Signal to Noise Ratio (SNR) as our metric which is ratio of mean squared value true position and MSE loss of predicted and true value of beam position of all the frames. For a very good model the SNR value should be higher.

$$\textbf{Signal to Noise Ratio (SNR)} = \frac{\sum_{\text{Frames}} (\text{True Position})^2}{\sum_{\text{Frames}} (\text{Predicted Position - True Position})^2} \tag{10}$$

7.4 Optimizer

We have chosen Adaptive Moment (Adam) as optimizer for our purpose. Optimizer helps us to reach at the optimised values of the weights. Adam is modified gradient descent method which finds the weights faster.

7.5 Hyperparameters

Batchsize: Instead of using the whole large training set at a time, we divide the data set into smaller sets called batches. The length of the these batches is called batchsize which is taken 32 in our problem.

Learning Rate: Here for Adam optimizer we are using a learning rate of 0.001. This learning rate defines how far away is your new weights from previous weights.

Learning Rate Scheduler: We are decreasing our learning rate by a factor of 2 after each 10 epochs. Changing learning rate with time helps to reach at the optimal solution faster by reducing overshooting.

Epochs: We are using 50 epochs i.e. training the model on train dataset 50 times.

8 Results

We have obtained following results for each of the simulation models after training the above discussed CNN model. Here we will show the difference between predicted position and true position of different frames of our test datasets. All of the positions are measured in centimeters. And corresponding histograms of residues have also been plotted in terms of fractional pixel error where 1 pixel = $\frac{34}{512}$=0.066 cm.

8.1 Gaussian Beam

8.1.1 Movement along X axis only

- Mean Squared Error: $3.85 \times 10^{-8}\text{cm}^2$
- Signal to Noise Ratio: 3236578.25

8.1.2 Movement along Y axis only

- Mean Squared Error: $4.26 \times 10^{-7}\text{cm}^2$
- Signal to Noise Ratio: 292608.21

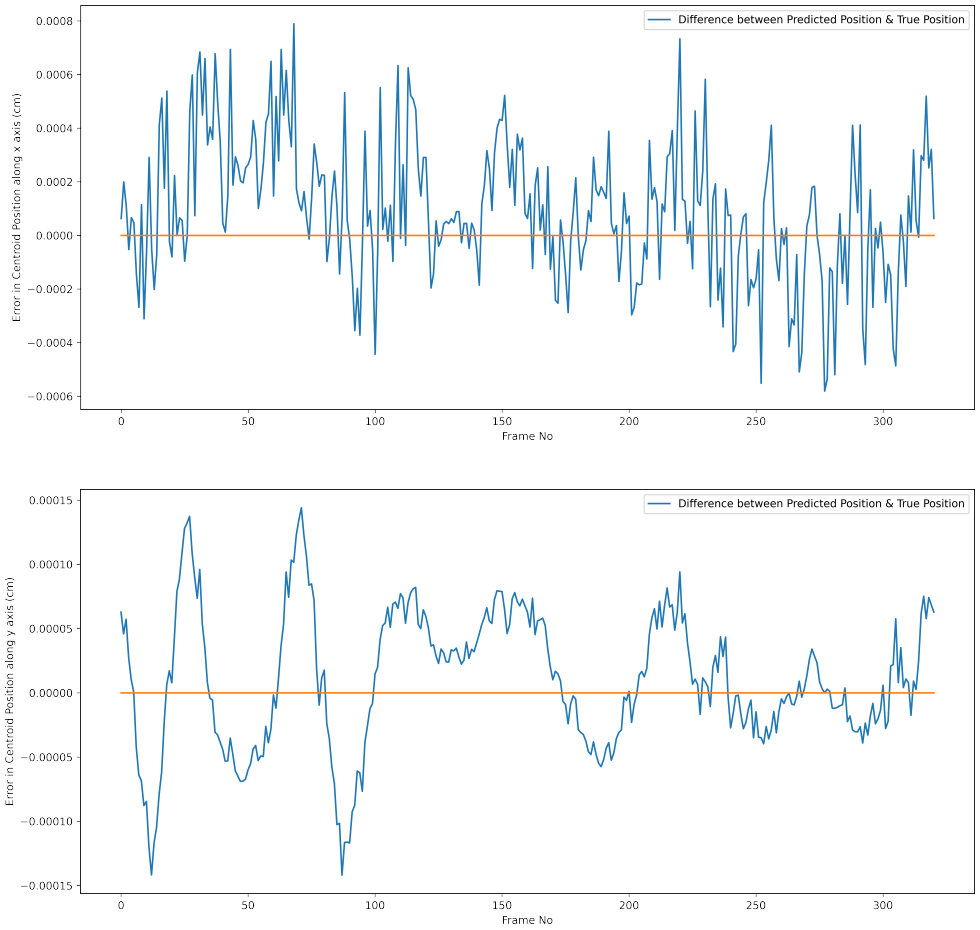

Figure 17: Difference between predicted position and true position for gaussian beam simulation model

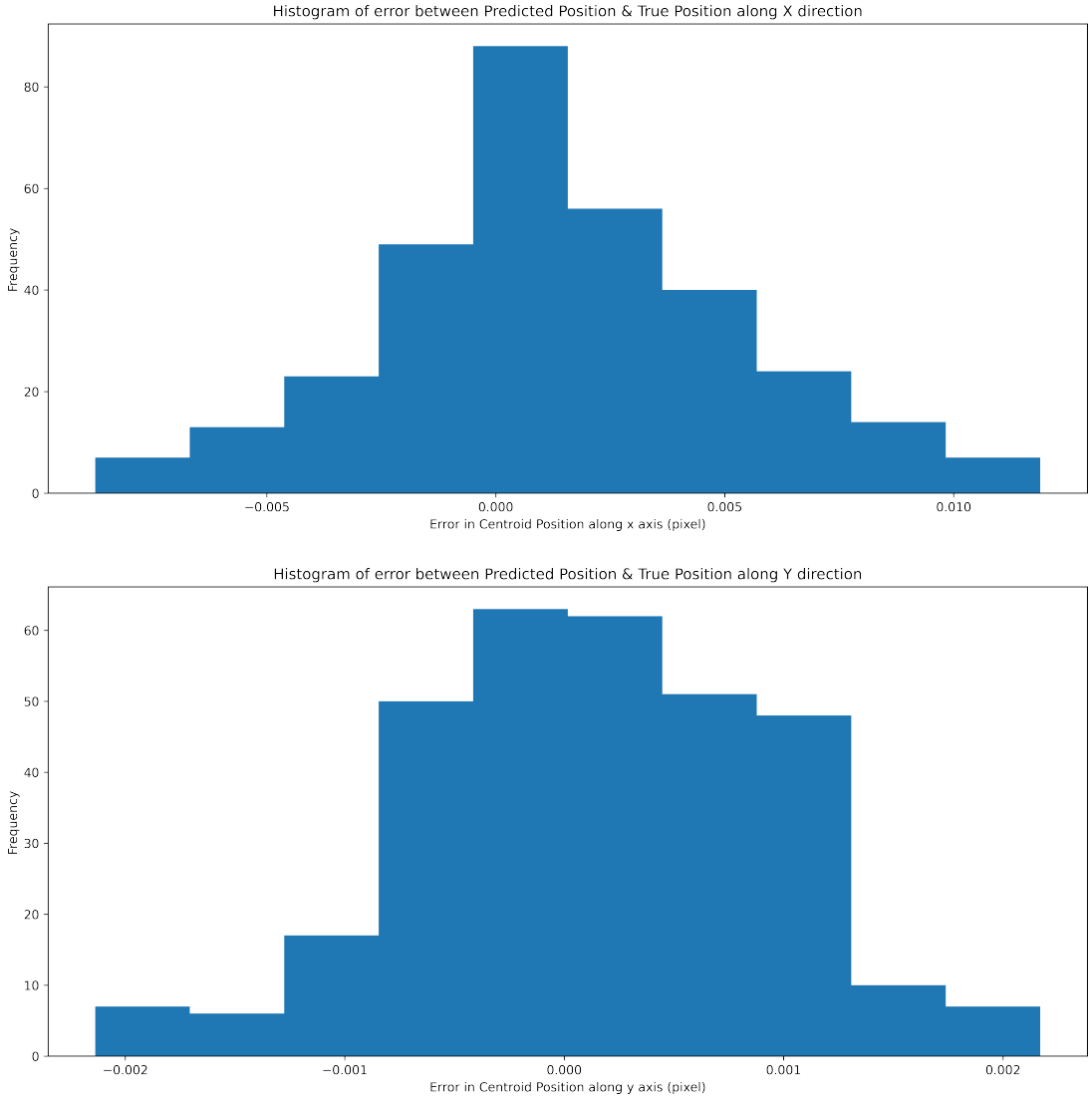

Figure 18: Histogram of error in centroid detection for gaussian beam simulation model

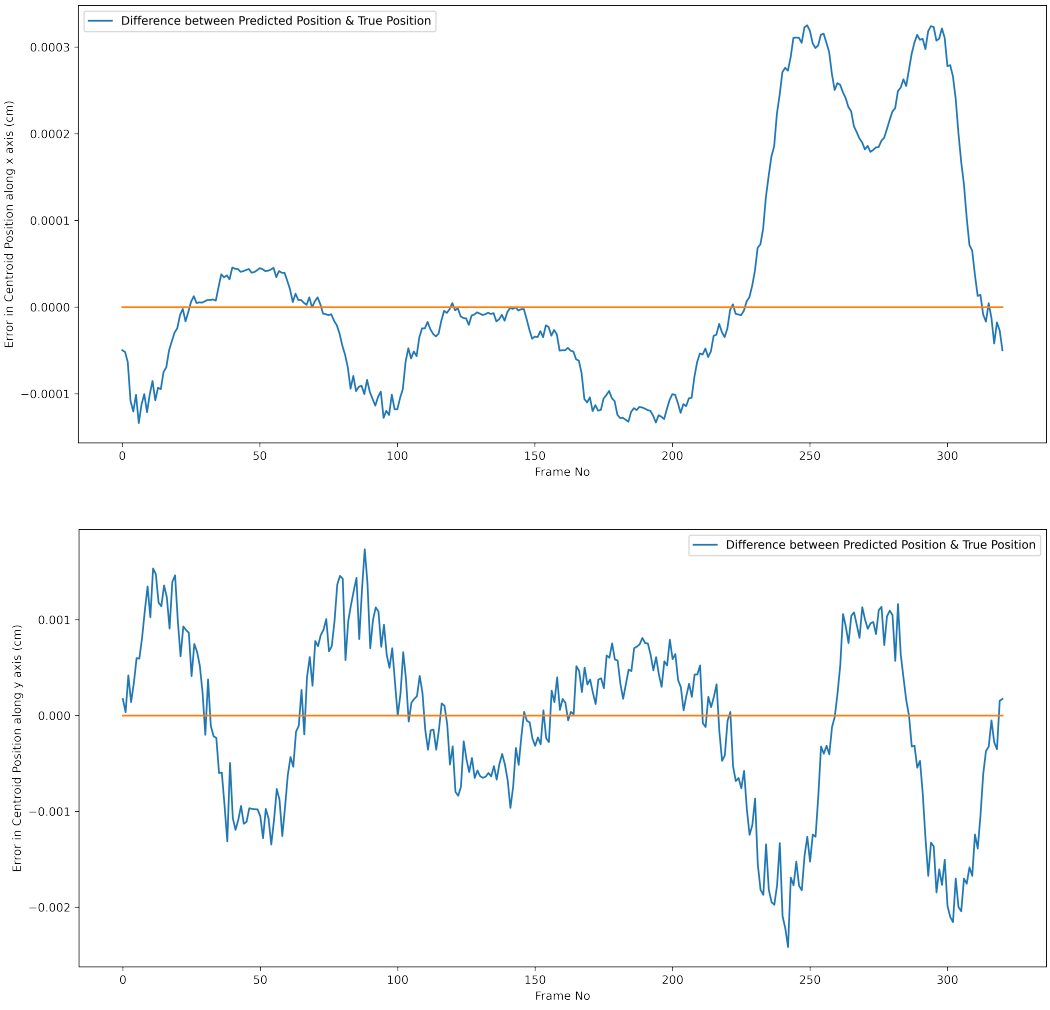

Figure 19: Difference between predicted position and true position for gaussian beam simulation model

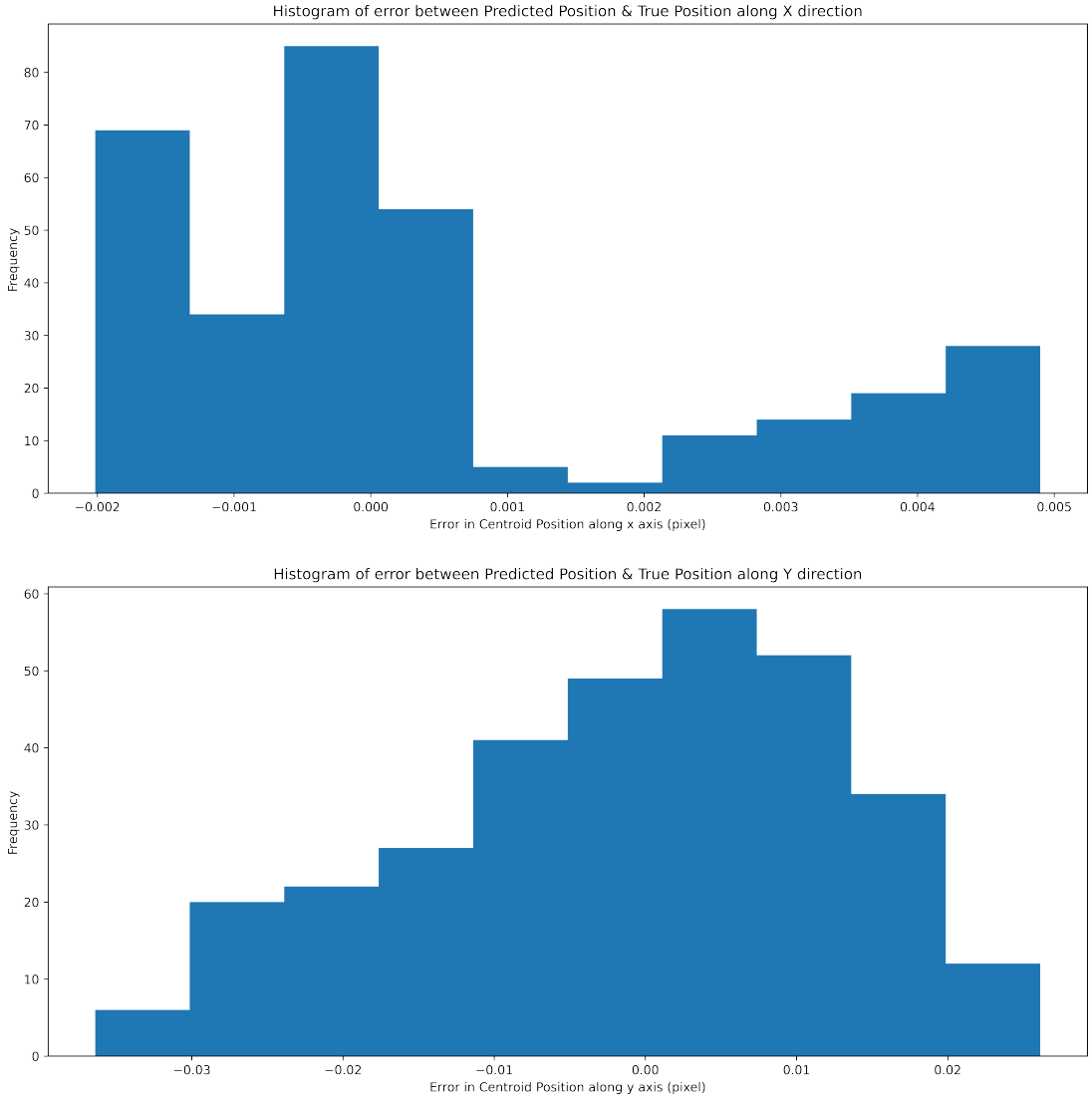

Figure 20: Histogram of error in centroid detection for gaussian beam simulation model

8.1.3 Movement on X-Y plane

- Mean Squared Error: $1.49 \times 10^{-6}\text{cm}^2$
- Signal to Noise Ratio: 250350.57

Figure 21: Difference between predicted position and true position for gaussian beam simulation model

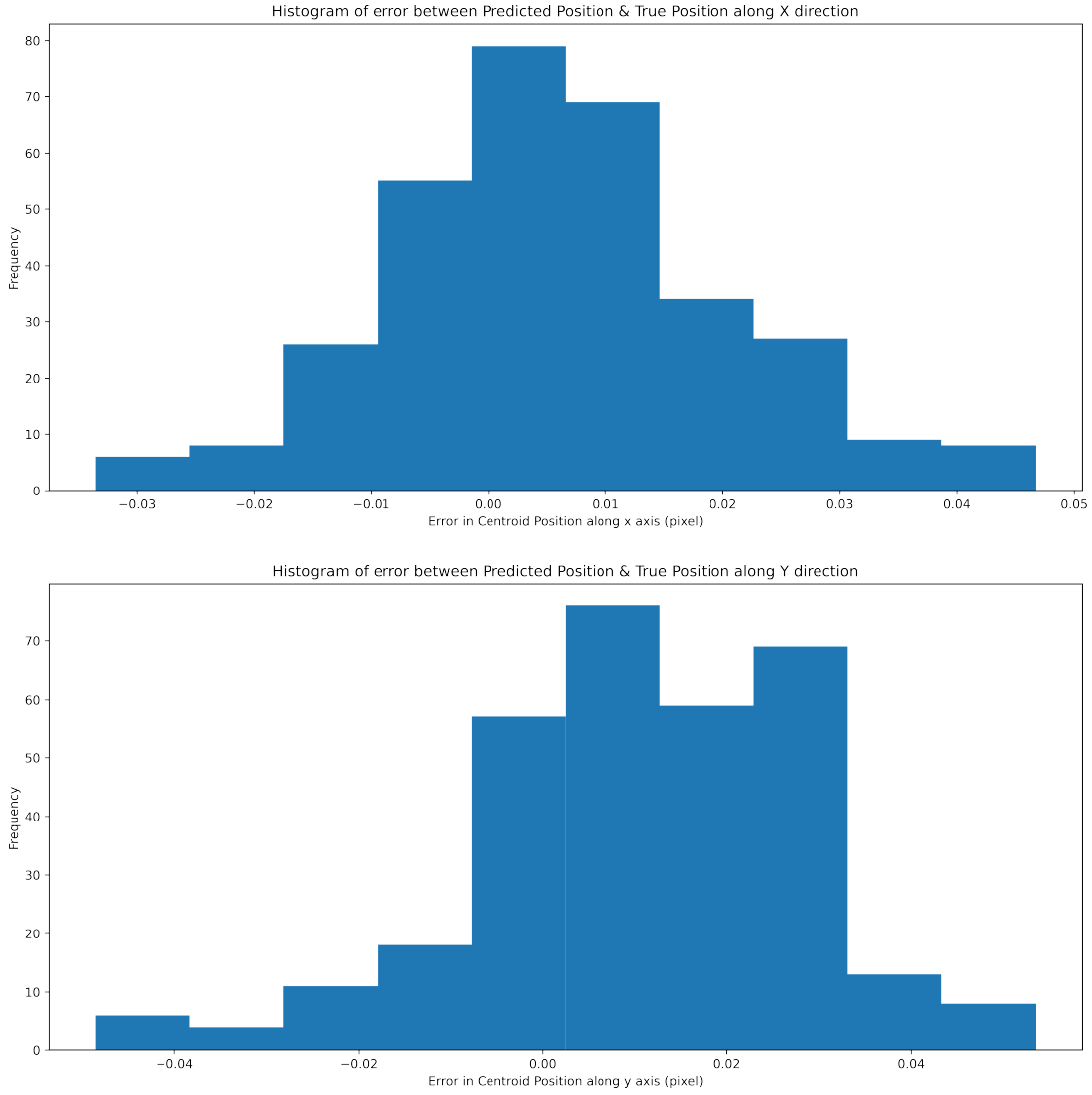

Figure 22: Histogram of error in centroid detection for gaussian beam simulation model

8.2 Scattered Beam

8.2.1 Movement along X axis only

- Mean Squared Error: $9.47 \times 10^{-7}\text{cm}^2$
- Signal to Noise Ratio: 131575.43

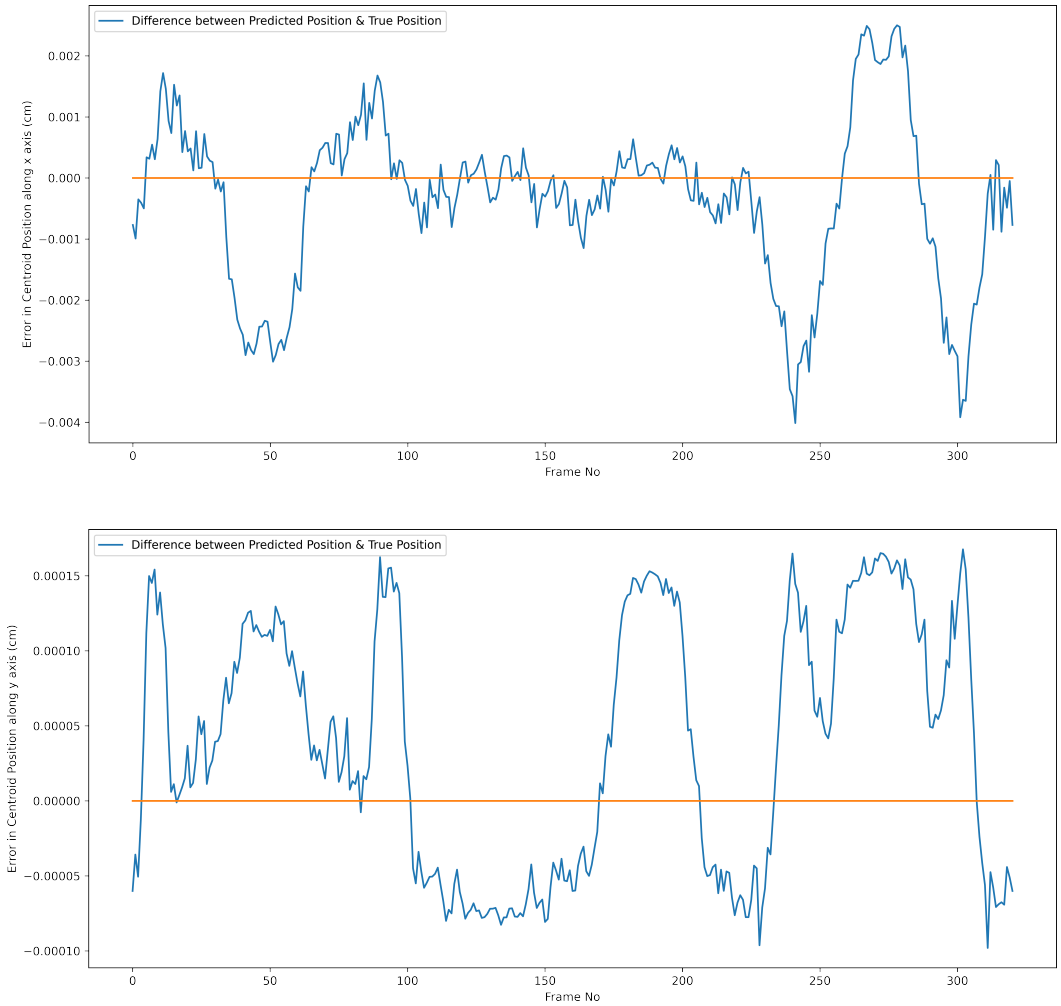

Figure 23: Difference between predicted position and true position for scattered beam simulation model

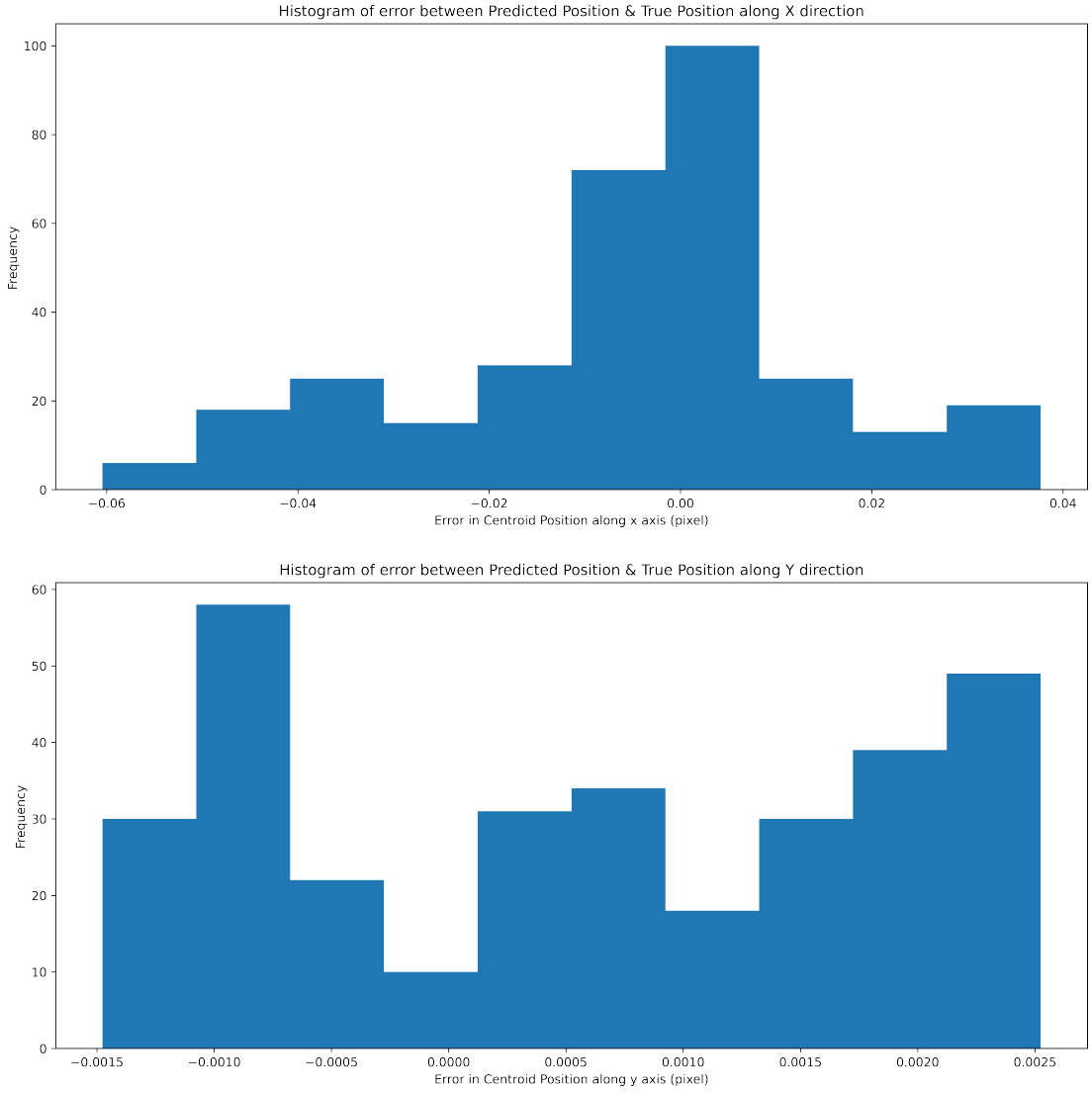

Figure 24: Histogram of error in centroid detection for scattered beam simulation model

8.2.2 Movement along Y axis only

- Mean Squared Error: $6.2 \times 10^{-7}\text{cm}^2$
- Signal to Noise Ratio: 200848.31

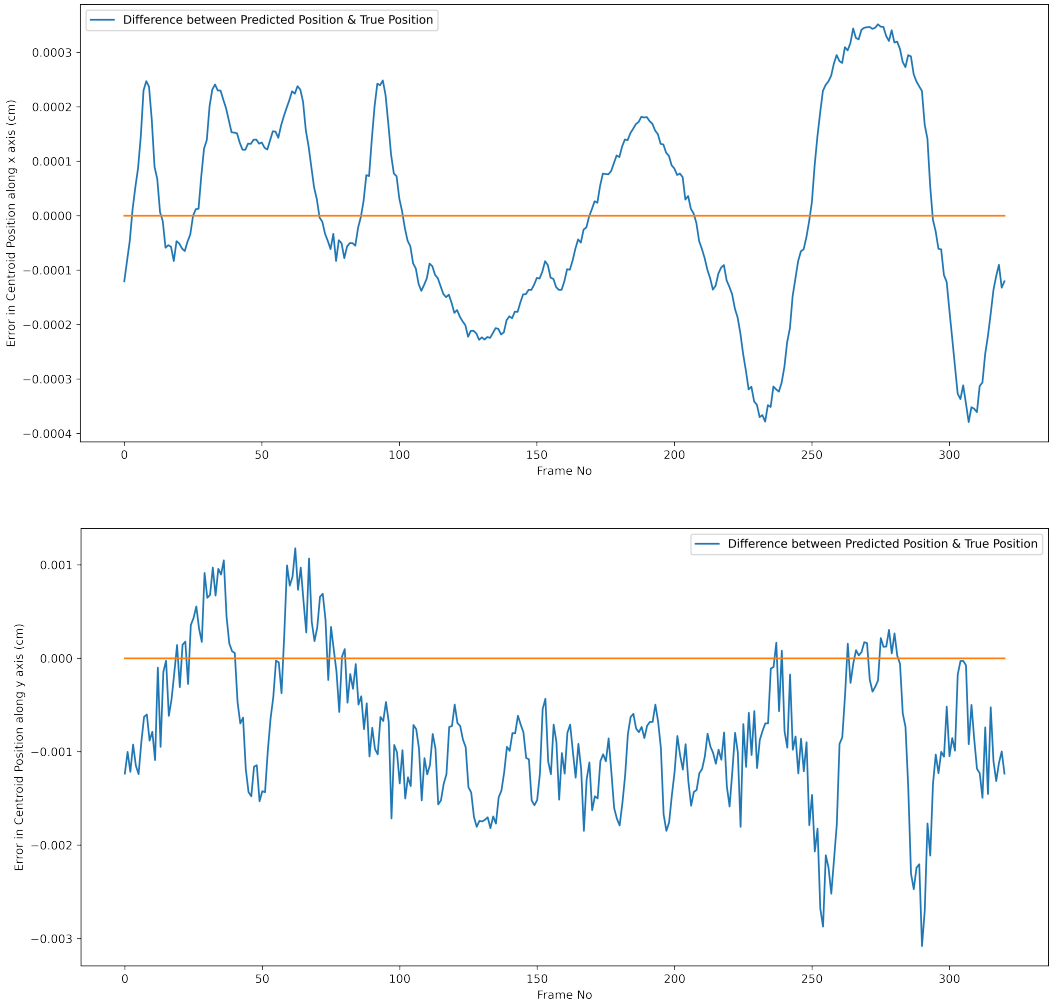

Figure 25: Difference between predicted position and true position for scattered beam simulation model

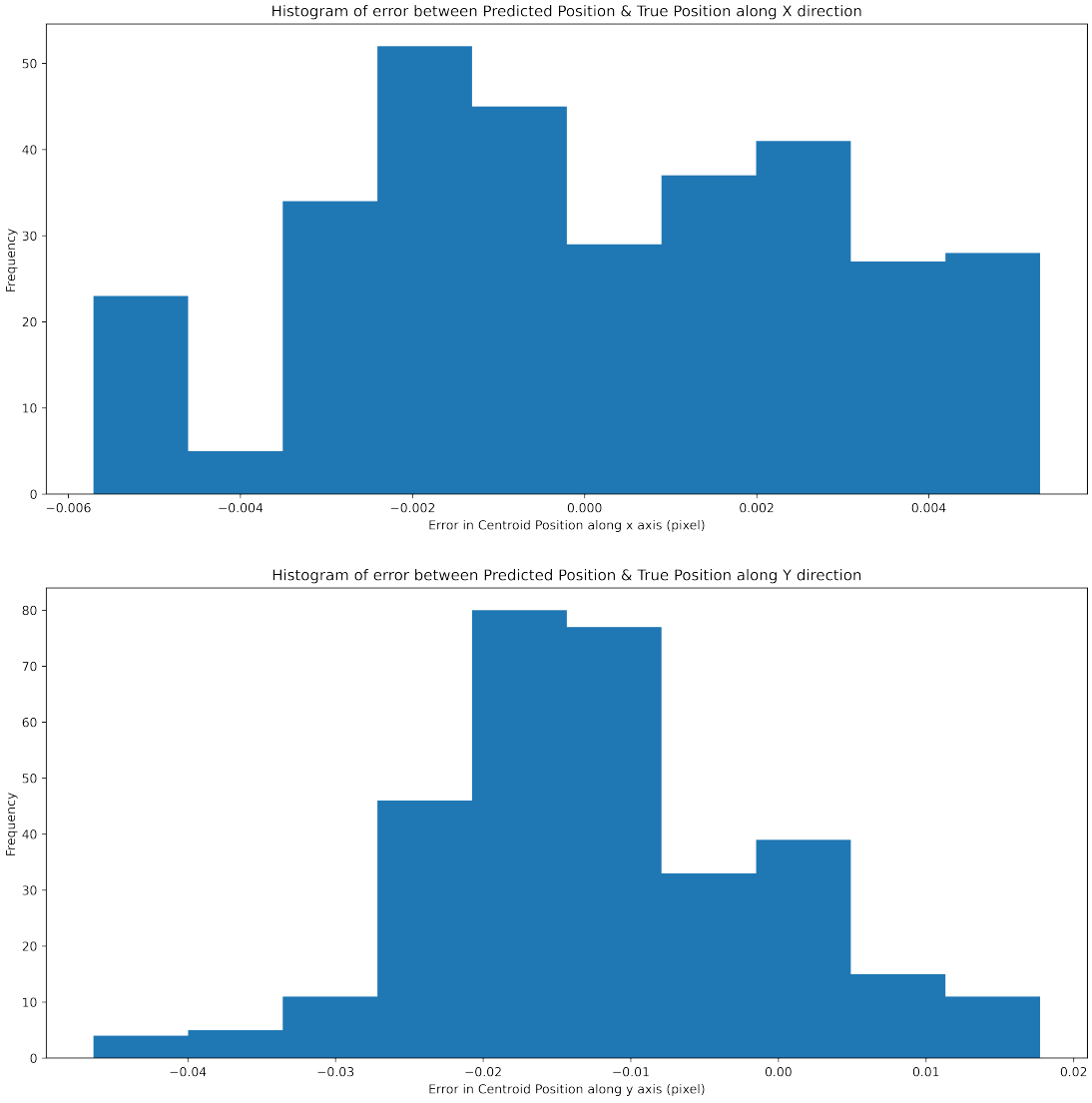

Figure 26: Histogram of error in centroid detection for scattered beam simulation model

8.2.3 Movement on X-Y Plane

- Mean Squared Error: $1.59 \times 10^{-6}\text{cm}^2$
- Signal to Noise Ratio: 235496.26

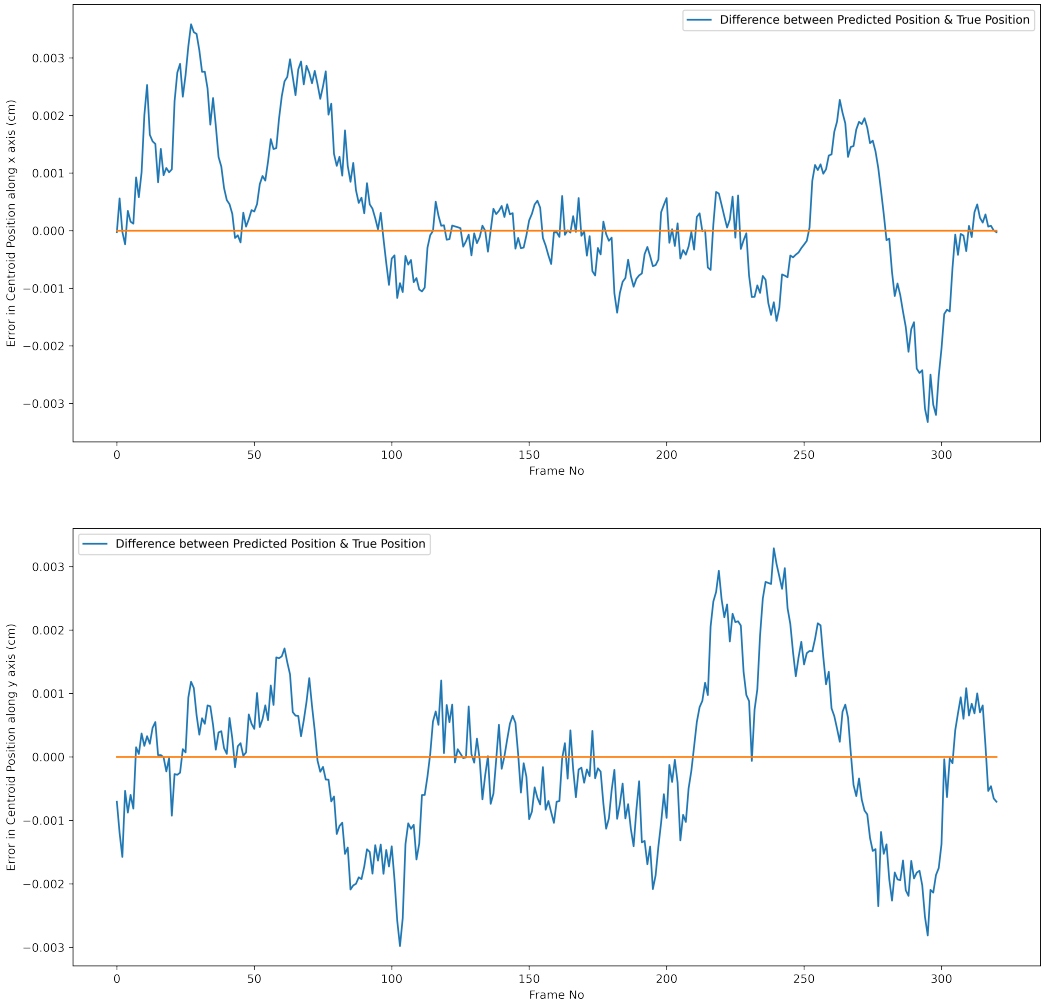

Figure 27: Difference between predicted position and true position for scattered beam simulation model

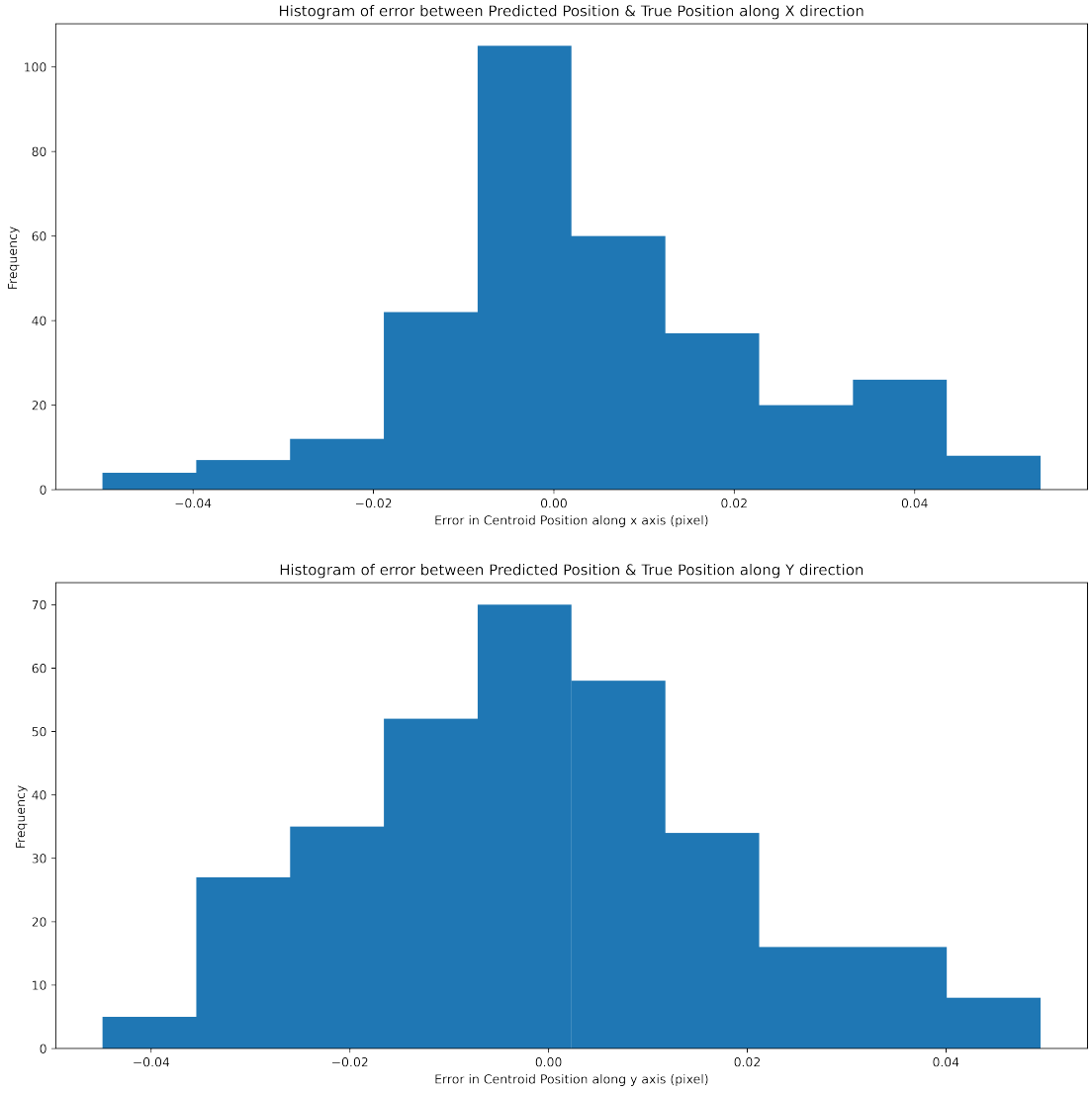

Figure 28: Histogram of error in centroid detection for scattered beam simulation model

8.3 Gaussian Beam with CCD Noise

8.3.1 Movement along X axis only

- Mean Squared Error: $1.92 \times 10^{-7}\text{cm}^2$
- Signal to Noise Ratio: 646445.21

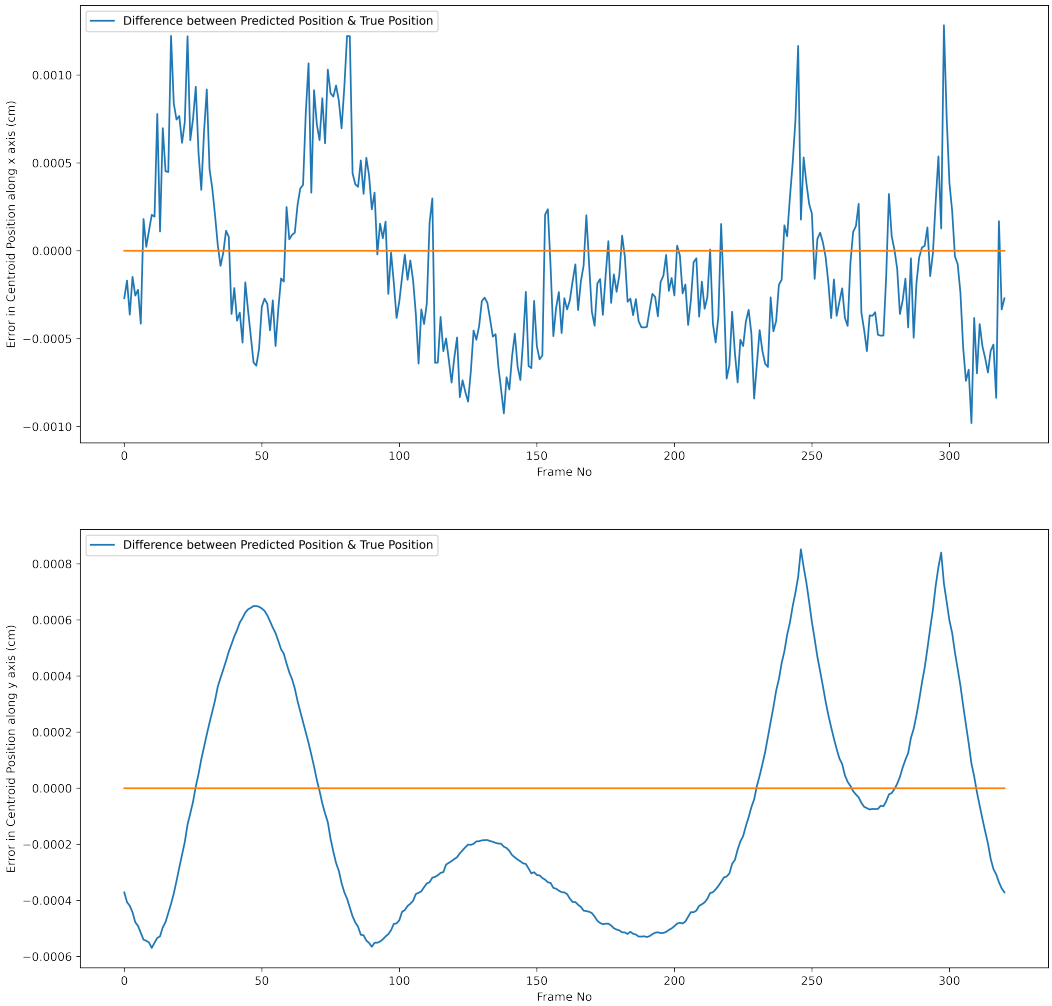

Figure 29: Difference between predicted position and true position for gaussian beam with CCD noise simulation model

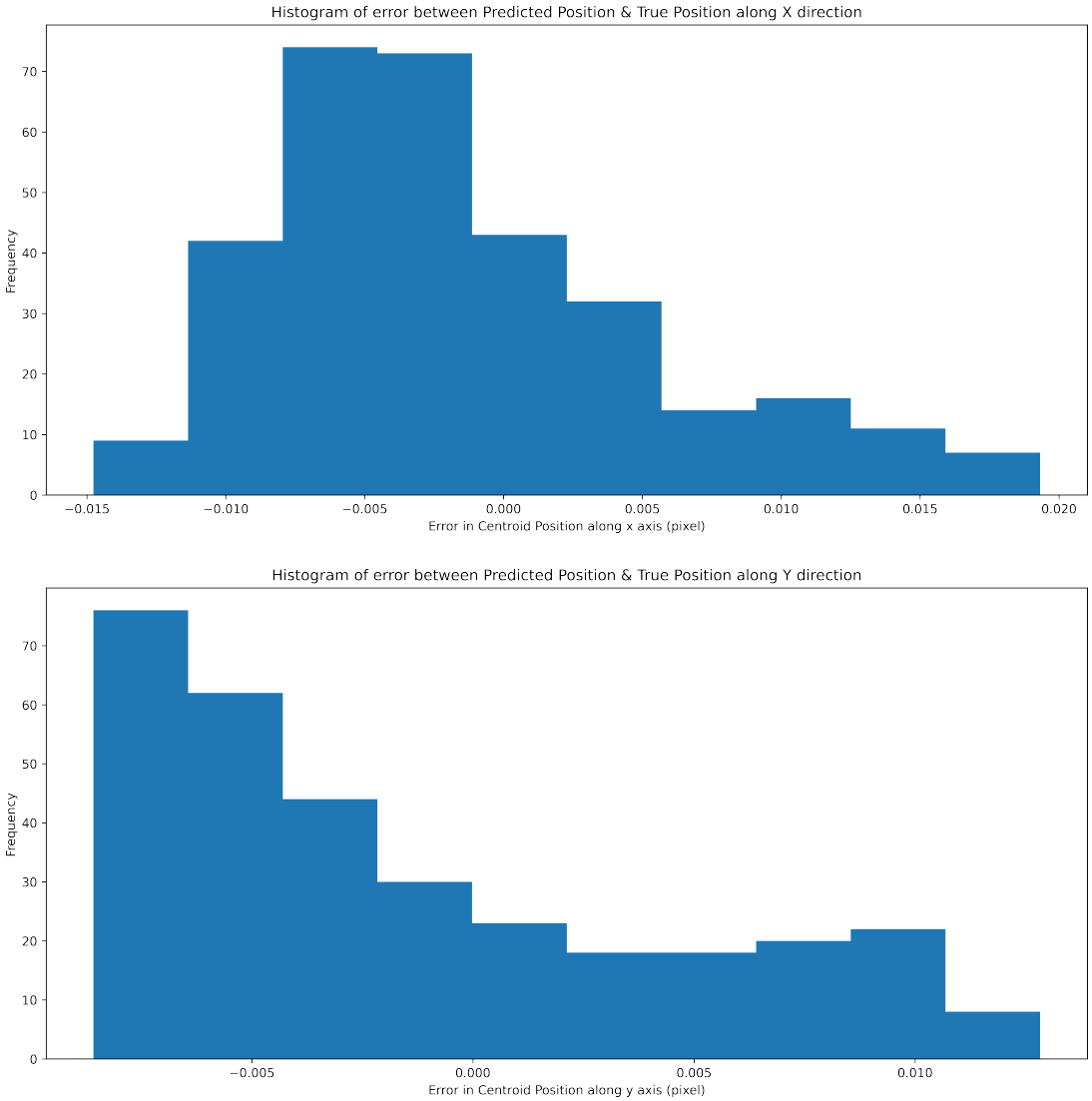

Figure 30: Histogram of error in centroid detection for gaussian beam with CCD noise simulation model

8.3.2 Movement along Y axis only

- Mean Squared Error: $2.42 \times 10^{-7}\text{cm}^2$
- Signal to Noise Ratio: 513956.71

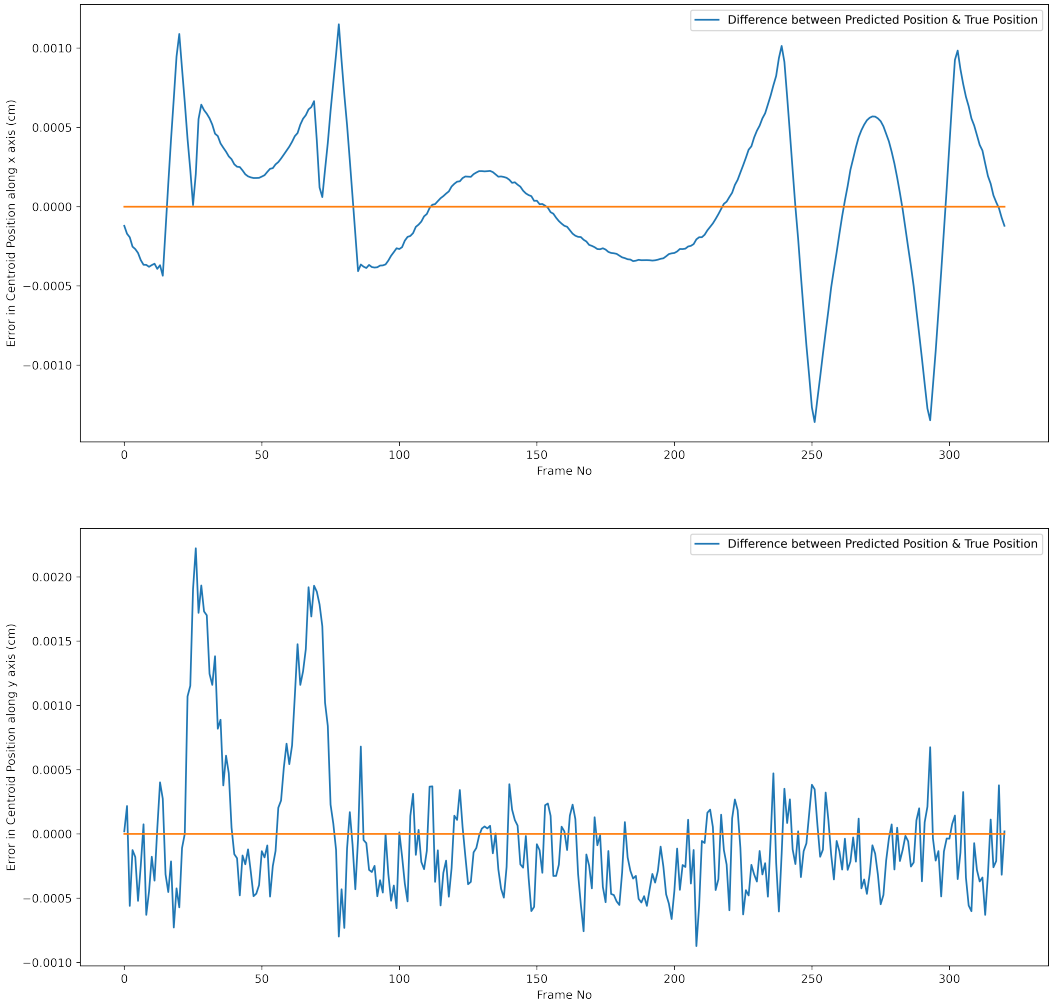

Figure 31: Difference between predicted position and true position for gaussian beam with CCD noise simulation model

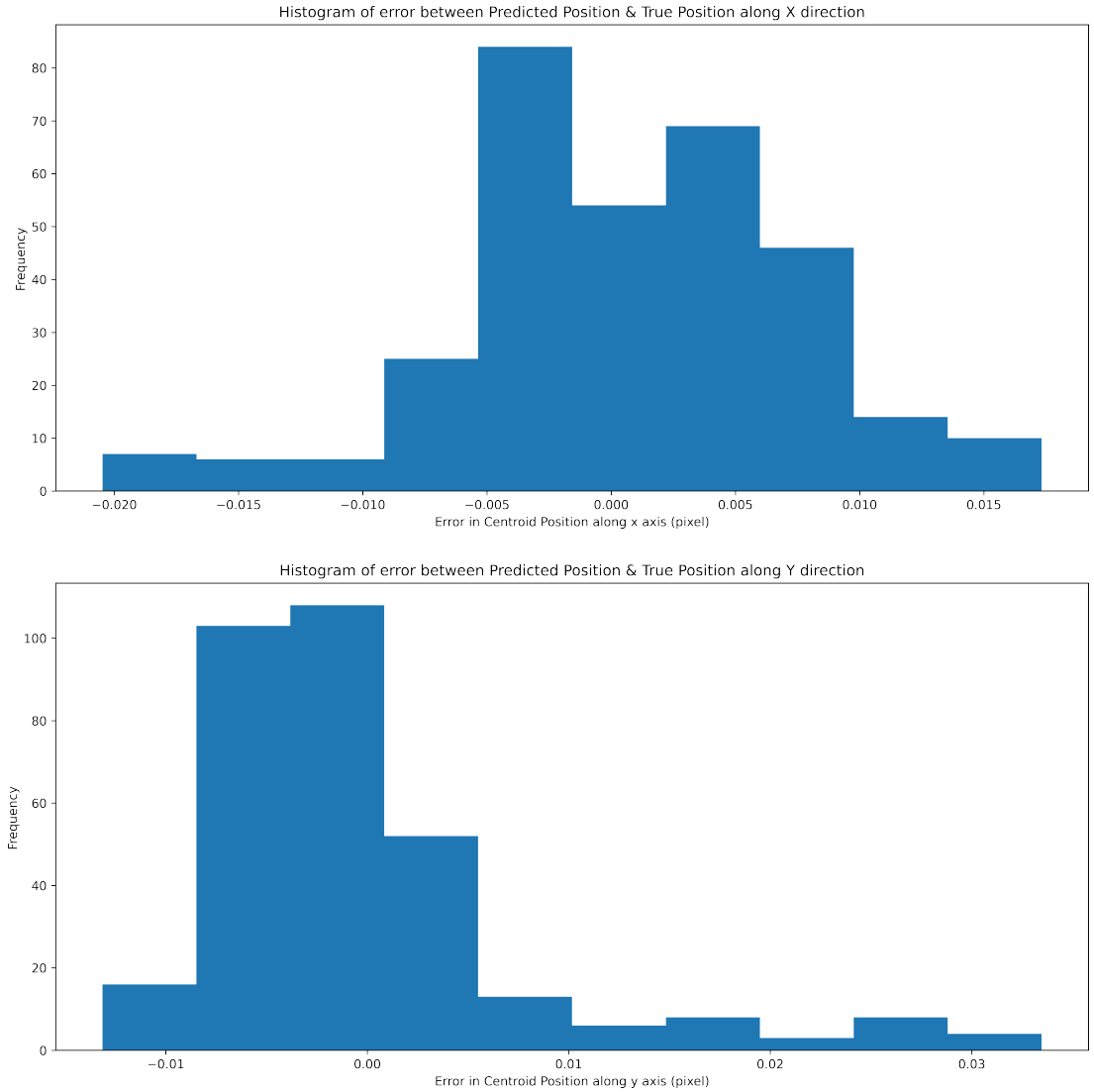

Figure 32: Histogram of error in centroid detection for gaussian beam with CCD noise simulation model

8.3.3 Movement on X-Y Plane

- Mean Squared Error: $8.26 \times 10^{-7}\text{cm}^2$
- Signal to Noise Ratio: 452277.76

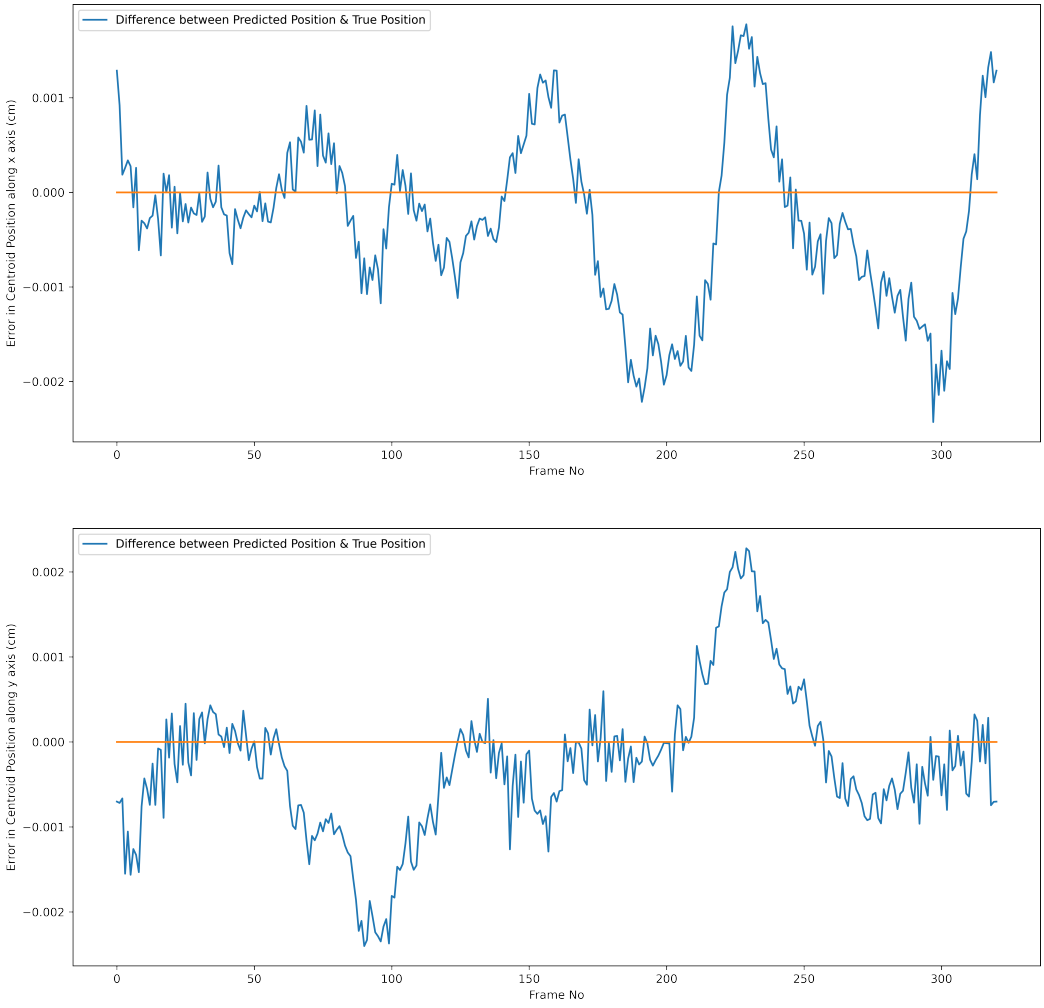

Figure 33: Difference between predicted position and true position for gaussian beam with CCD noise simulation model

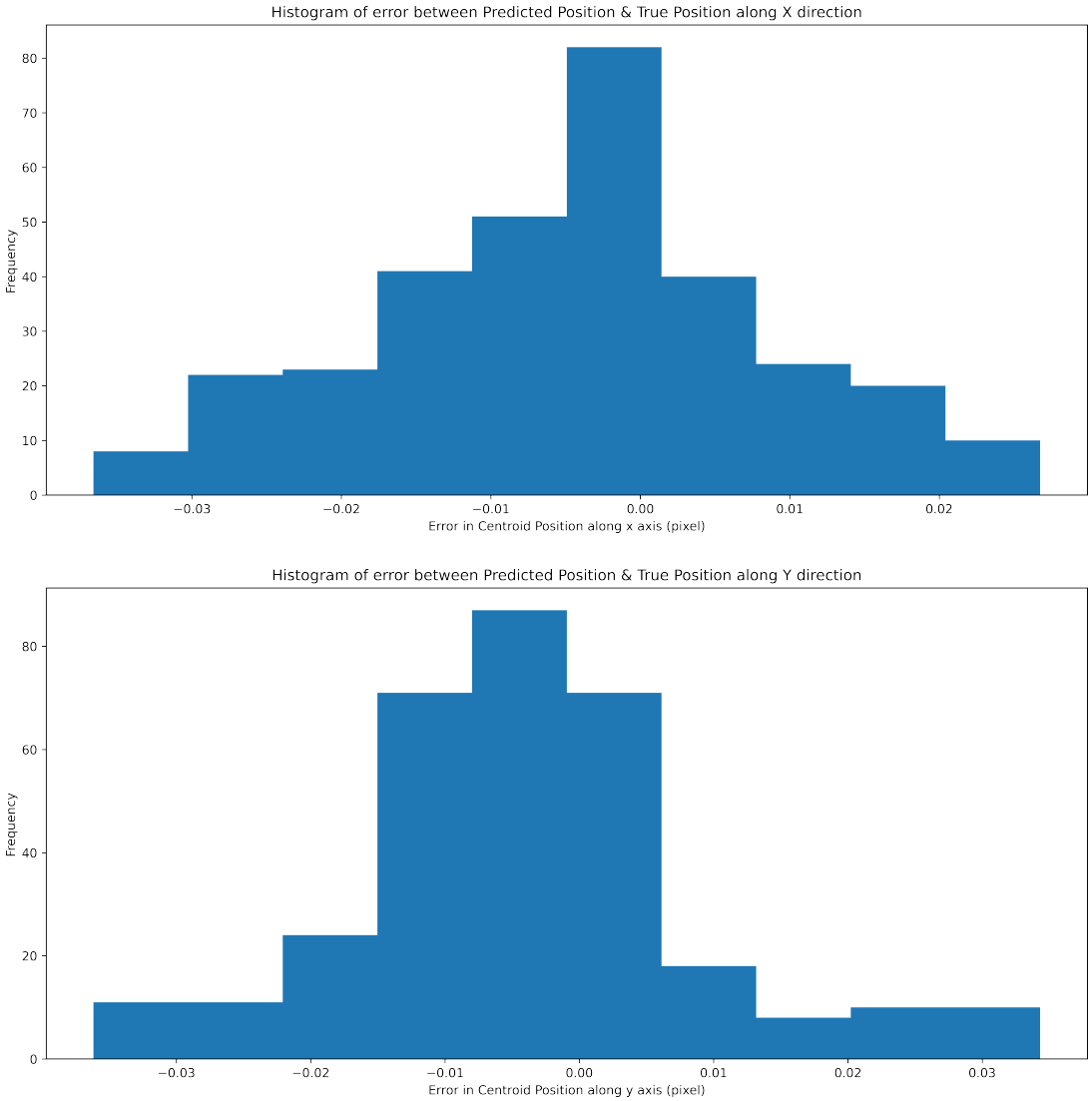

Figure 34: Histogram of error in centroid detection for gaussian beam with CCD noise simulation model

8.4 Scattered Beam with CCD Noise

8.4.1 Movement along X axis only

- Mean Squared Error: $7.28 \times 10^{-7}\text{cm}^2$
- Signal to Noise Ratio: 171082.57

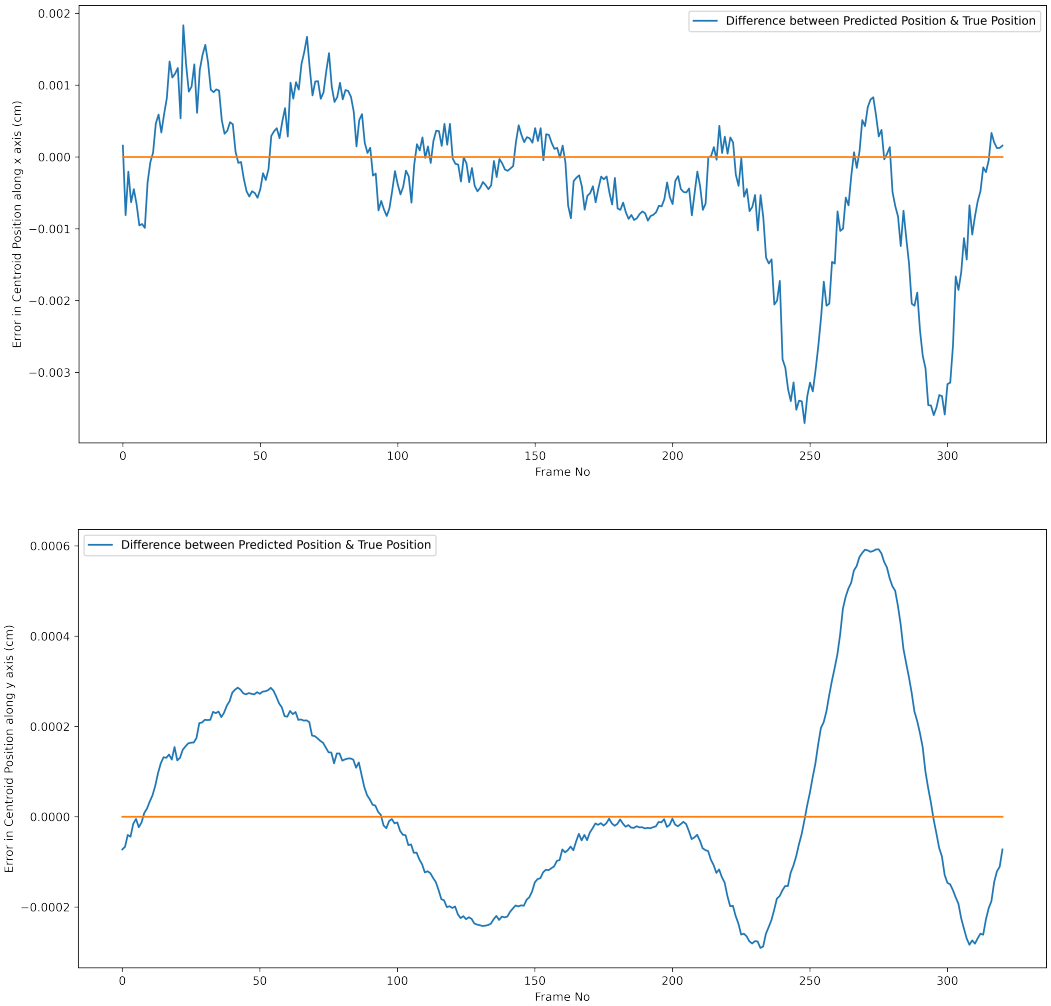

Figure 35: Difference between predicted position and true position for scattered beam with CCD noise simulation model

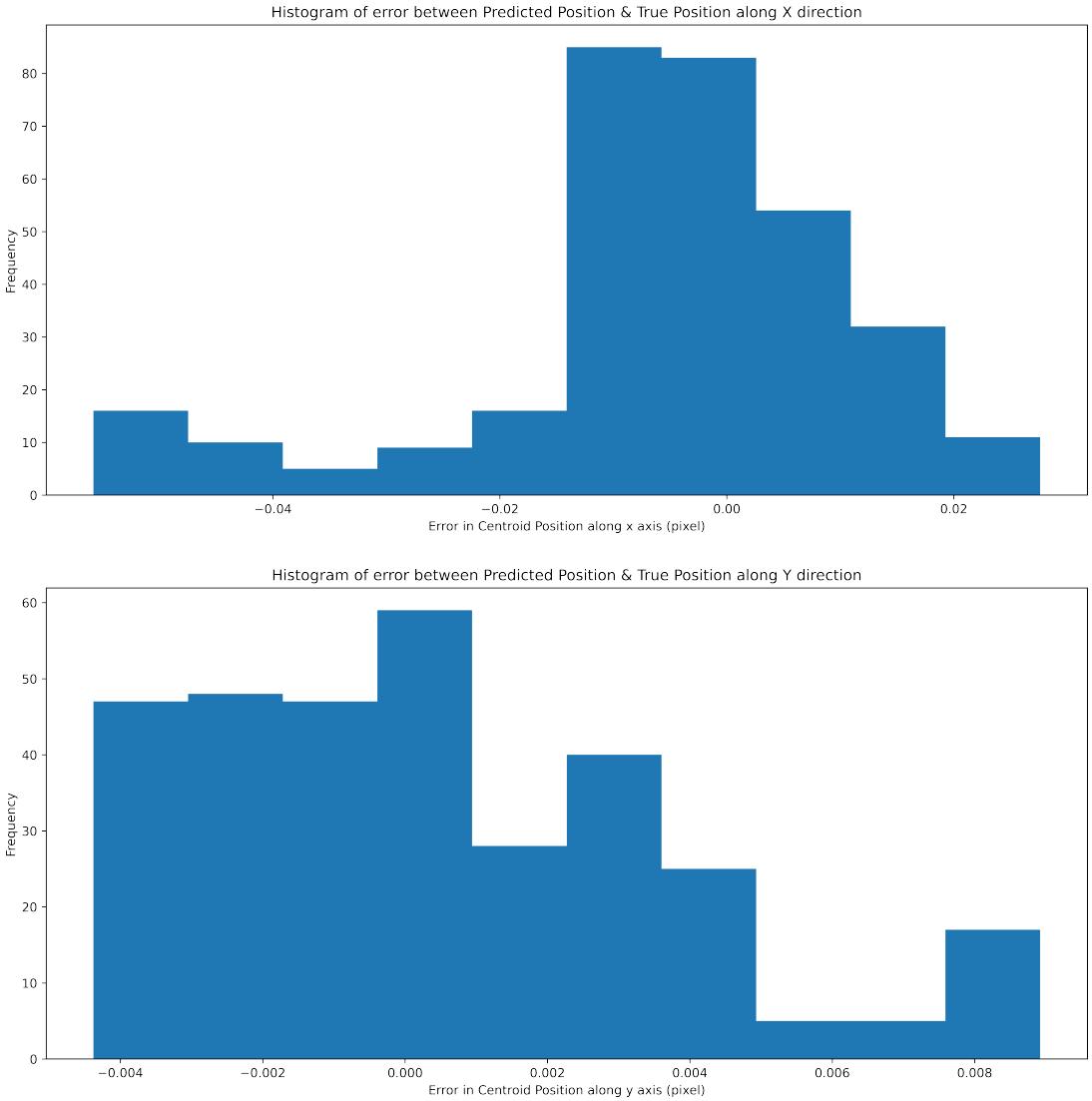

Figure 36: Histogram of error in centroid detection for scattered beam with CCD noise simulation model

8.4.2 Movement along Y axis only

- Mean Squared Error: $2.46 \times 10^{-7}\text{cm}^2$
- Signal to Noise Ratio: 506563.46

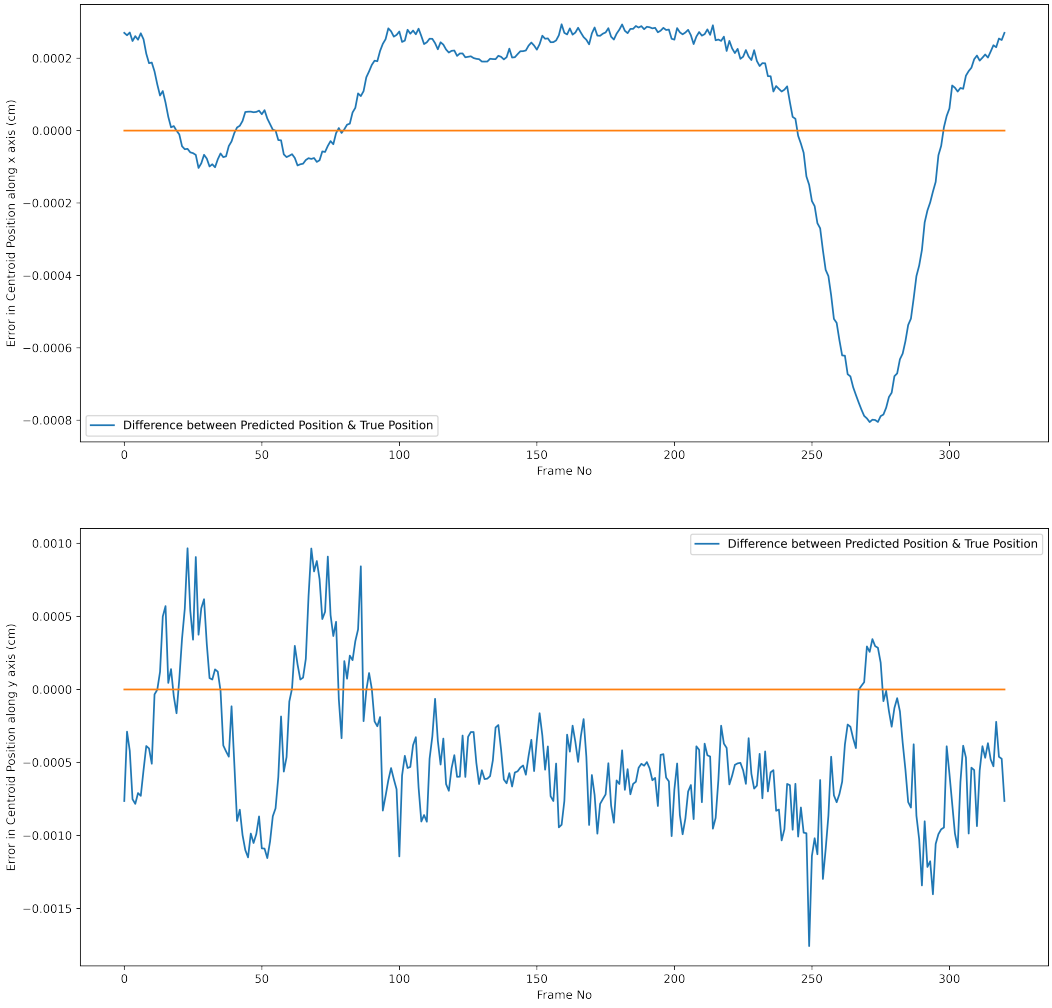

Figure 37: Difference between predicted position and true position for scattered beam with CCD noise simulation model

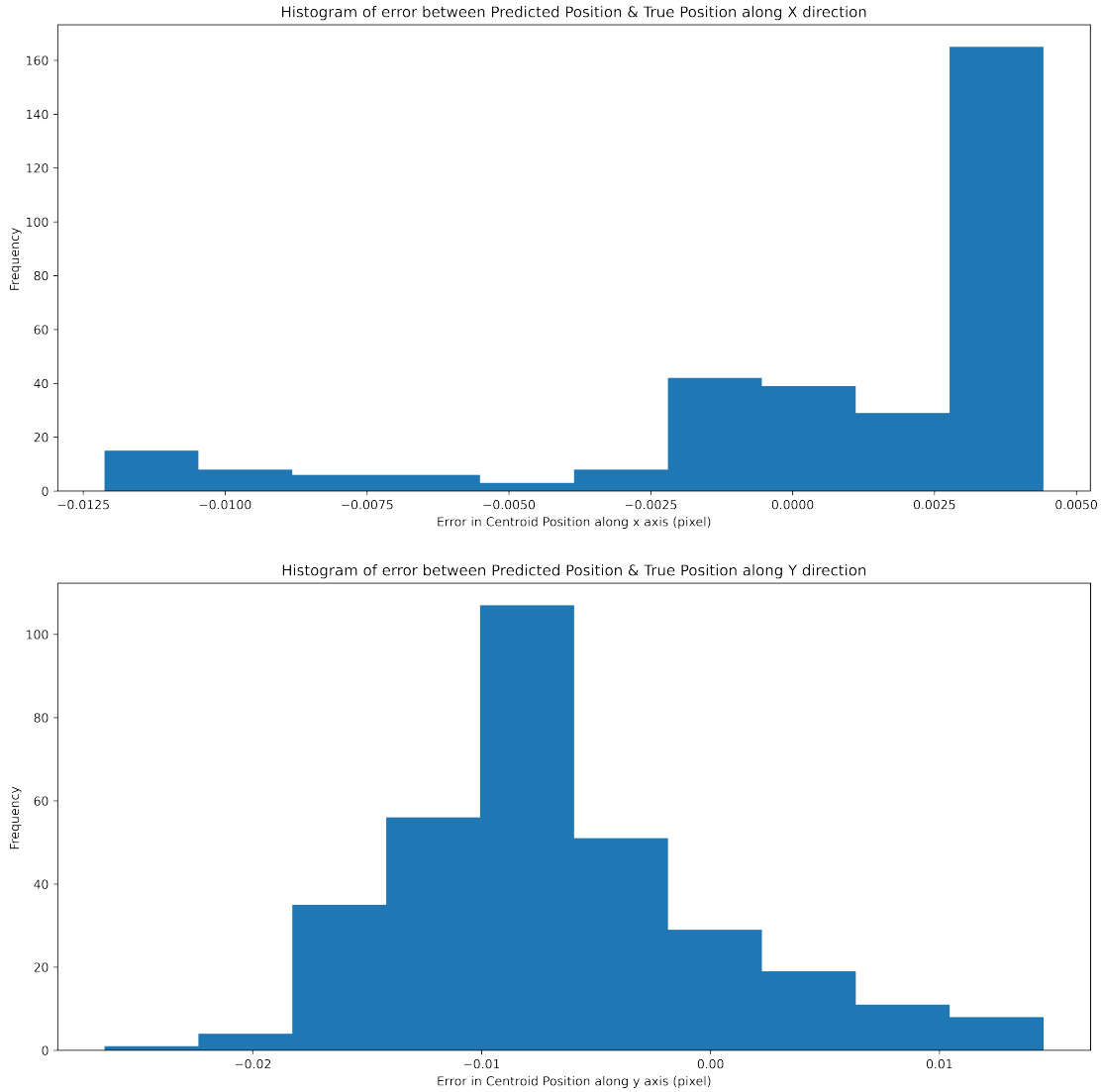

Figure 38: Histogram of error in centroid detection for scattered beam with CCD noise simulation model

8.4.3 Movement on X-Y Plane

- Mean Squared Error: $1.87 \times 10^{-6}\text{cm}^2$
- Signal to Noise Ratio: 199444.28

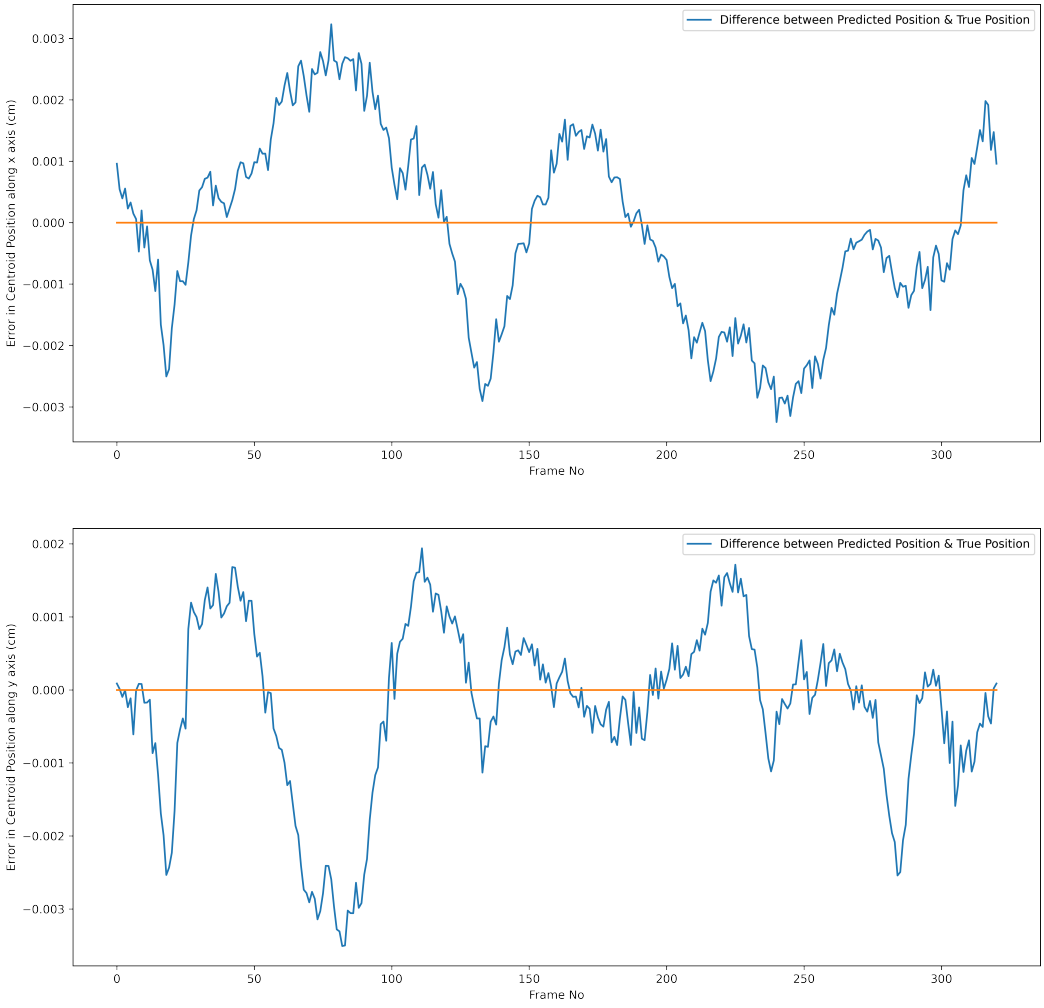

Figure 39: Difference between predicted position and true position for scattered beam with CCD noise simulation model

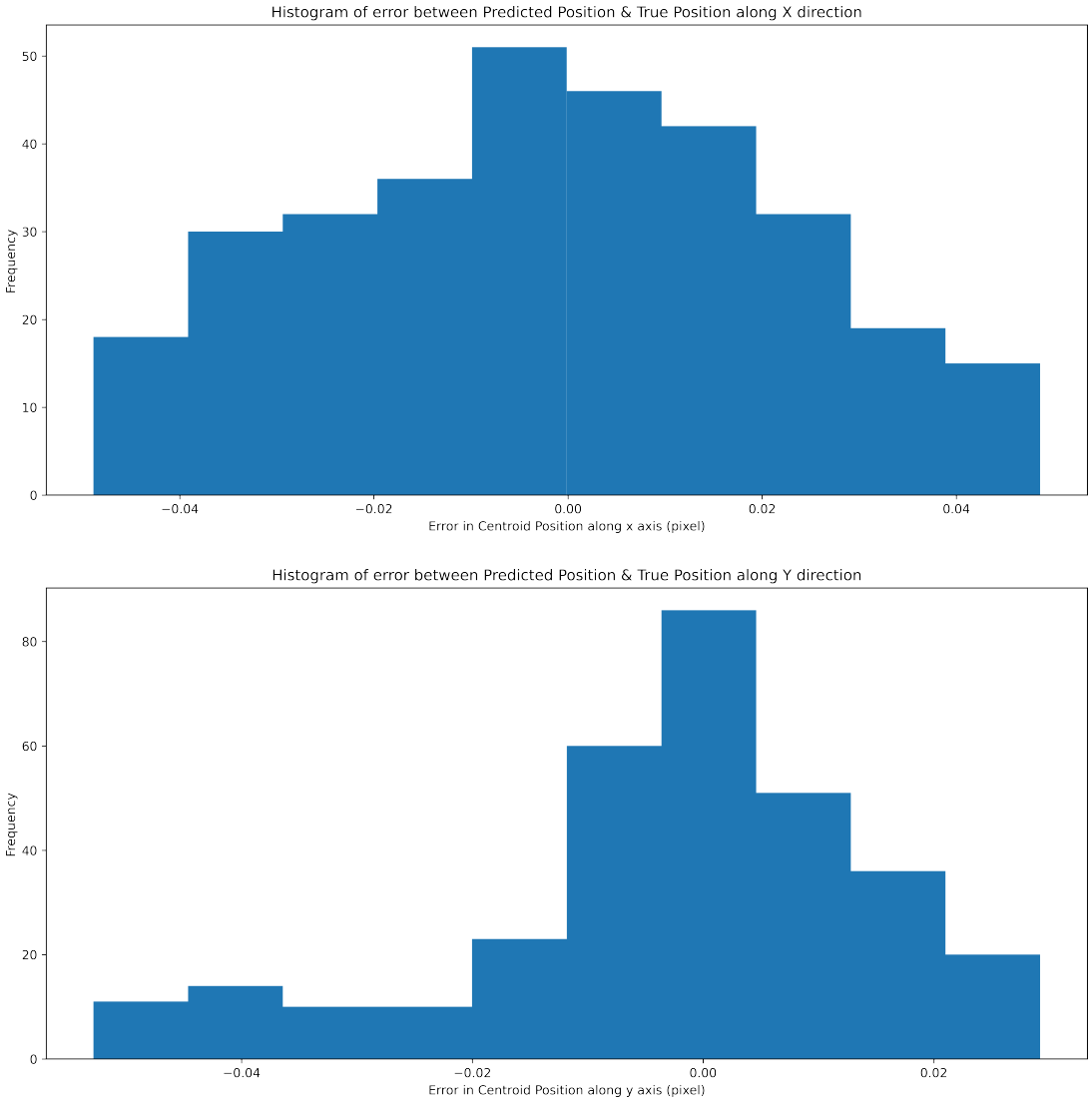

Figure 40: Histogram of error in centroid detection for scattered beam with CCD noise simulation model

9 Conclusion

Finally we have been able to reach sub pixel accuracy. Our model can detect the position of the beam spot with a maximum error of 40 micron. In future I am planning to run this CNN model on simulation models contatining point scatterers and expecting to develop more realistic models. This time I have not got the scope of working with real labeled data. Perhaps in near future I will try to run it on real dataset.

10 Acknowledgement

I am thankful to Prof. Rana Adhikari, Dr. Yehonathan Drori, Dr. Tega Edo for guiding me throughout this summer. A special thanks to Prof. Alan Weinstein for hosting the LIGO SURF programme and conducting lectures on various topics. I would like to thank other SURF students for making this a memorable summer. This list will be incomplete without mentioning Prof. Sayan Kar whose guidance has brought me to this place and thanks to my teachers, profs for making me the person who I am today. At last I would like to show my gratitute to all members of Caltech LIGO Group, National Science Foundation (NSF), LIGO India who have played a key role in enriching this experience.

References

[1] Milind Kumar Vaddiraju, Mentors: Rana Adhikari, Gautam Venugopalan, Koji Arai, *Laser beam position tracking for LIGO interferometers*. LIGO-SURF Report (2019).

[2] Kruthi Krishna, Mentors: Gautam Venugopalan, Koji Arai, Rana Adhikari, *High FidelityProbe of Optical Scatter from Point Defects*. LIGO-SURF Report (2019).

[3] https://www.baslerweb.com/fp-1489067421/media/downloads/documents/emva_data/BD00084701_Basler_acA640-120gm_AHR-SGP_EMVA_Standard_1288.pdf

[4] http://blue.ligo-wa.caltech.edu:8000/40m/40mHomePage